JACS
JOURNAL OF THE AMERICAN CHEMICAL SOCIETY

ARTICLE

pubs.acs.org/JACS

Main-Chain Boron-Containing Oligophenylenes via Ring-Opening Polymerization of 9-H-9-Borafluorene

Alexander Hübner,[†] Zheng-Wang Qu,[†] Ulli Englert,[‡] Michael Bolte,[†] Hans-Wolfram Lerner,[†] Max C. Holthausen,[*,†] and Matthias Wagner[*,†]

[†]Institut für Anorganische und Analytische Chemie, Johann Wolfgang Goethe-Universität Frankfurt, Max-von-Laue-Strasse 7, D-60438 Frankfurt am Main, Germany.

[‡]Department of Inorganic Chemistry, RWTH Aachen, Landoltweg 1, D-52056 Aachen.

Supporting Information

ABSTRACT: 9-H-9-Borafluorene ($H_8C_{12}BH$; **5**) can be generated in situ from 9-Br-9-borafluorene and Et_3SiH in benzene or hexane. Monitoring of the reaction by NMR spectroscopy at rt in C_6D_6 reveals that **5** forms C_1-symmetric dimers $(\mathbf{5})_2$ under these conditions. DFT calculations on conceivable isomers of $(\mathbf{5})_2$ and a comparison of calculated and experimentally determined ^1H, ^{13}C, and ^{11}B NMR shift values lead to the conclusion that $(\mathbf{5})_2$ is not a classical dimer $H_8C_{12}B(\mu\text{-}H)_2BC_{12}H_8$, but contains one B−H−B three-center, two-electron bond together with a boron-bridging phenyl ring. Addition of 1 equiv of pyridine to $(\mathbf{5})_2$ leads to the clean formation of the pyridine adduct $H_8C_{12}BH(py)$ (**5·py**). Likewise, $(\mathbf{5})_2$ can be employed in hydroboration reactions, as evidenced by its transformation with 0.5 equiv of *tert*-butylacetylene, which gives the hydroboration products $tBuC(H)_2C(H)(BC_{12}H_8)_2$ (**9**) and $tBuC(H)C(H)BC_{12}H_8$ in almost quantitative yield. $(\mathbf{5})_2$ is not long-term stable in benzene solution. Addition of pyridine to aged reaction mixtures allowed the isolation of the adduct $(py)H_2B\text{-}C_6H_4\text{-}C_6H_4\text{-}(py)BC_{12}H_8$ (**10·py₂**) of a ring-opened dimer of **5**. Storage of a hexane solution of 9-Br-9-borafluorene and Et_3SiH for 1−2 weeks at rt leads to the formation of crystals of a ring-opened pentamer $H[\text{-}(H)B\text{-}(C_6H_4)_2\text{-}]_4BC_{12}H_8$ (**11**) of **5** (preparative yields are obtained after 1−4 months). The polymer main chain of **11** is reinforced by four intrastrand B−H−B three-center, two-electron bonds. Apart from the main product **11**, we have also isolated minor amounts of closely related oligomers carrying different chain ends, i.e., $H_8C_{12}B\text{-}(C_6H_4)_2[\text{-}(H)B\text{-}(C_6H_4)_2\text{-}]_2BC_{12}H_8$ (**12**) and $H[\text{-}(H)B\text{-}(C_6H_4)_2\text{-}]_5BH_2$ (**13**). When the reaction between 9-Br-9-borafluorene and Et_3SiH is carried out in refluxing toluene, the cyclic dimer $[\text{-}(\mu\text{-}H)B\text{-}(C_6H_4)_2\text{-}]_2$ (**14**) can be obtained in a crystalline yield of 25%. The compounds **9**, **10·py₂**, **11**, **12**, **13**, and **14** have been structurally characterized by X-ray crystallography. The entire reaction pathway leading from **5** to **10**, **11**, **12**, **13**, and **14** has been thoroughly elucidated by DFT calculations and we propose a general mechanistic scenario applicable for ring-opening polymerization reactions of 9-borafluorenes.

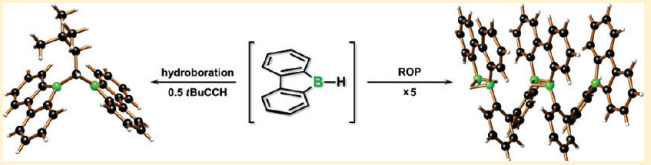

INTRODUCTION

Incorporation of the main group elements B, Si, N, P, or S into organic π-electron materials is a powerful approach to modifying the optical and electronic properties of the parent systems.[1] The consequent notion that classical inorganic solid-state materials can be replaced by lightweight and highly tunable organoelement compounds sparked a vibrant interest in this field of research.[2] In this context, boron has lately moved to the center stage of elements used as dopants for extended π-conjugated organic frameworks. Boron atoms can efficiently interact with organic π-systems through their vacant p-orbitals,[3,4] and as a result, the electronic structure of the material is modified with an impact on its optical and charge transport properties. Moreover, organoboranes possess a high Lewis acidity and can therefore engage in Lewis acid−base reactions. As a result of adduct formation, the local geometry about the boron center changes from trigonal-planar to tetrahedral so that π-conjugation pathways across the boron p-orbital are disrupted, which can be exploited for the design of molecular switches. Today, boron-doped π-systems are relevant for a broad range of applications as, e.g., luminophores and hole transporters in organic light-emitting devices, as components of organic solar cells, and as sensors for the detection of biologically or environmentally relevant anions.[2,5−8]

For the design of boron-containing π-conjugated polymers, two cases have to be distinguished, i.e., the boron atoms can either be introduced as lateral substituents or are incorporated as integral parts of the polymer main chain.[9,10] The dopant influence on the overall optoelectronic properties is maximized in the latter class of compounds but only a few synthetic strategies exist to prepare main-chain boron-containing π-conjugated systems. The most prominent are polycondensation approaches[11−18] and the hydroboration polymerization.[19−25]

Our group has recently reported on a novel polycondensation protocol, which takes advantage of the fact that

Received: December 6, 2010
Published: March 02, 2011

Scheme 1. π-Conjugated Polymers Synthesized by Polycondensation (2) and by Hydroboration Polymerization (4)

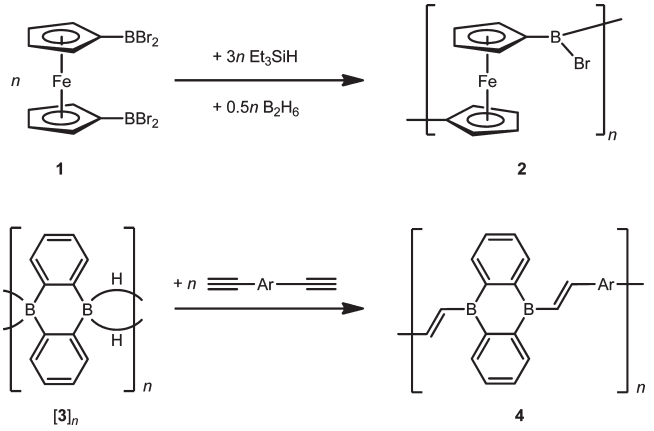

(organyl)(hydrido)boranes tend to undergo substituent scrambling reactions. In the particular case of 1,1′-bis(dibromoboryl)ferrocene (**1**; Scheme 1), a partial Br/H exchange with Et_3SiH induces the formation of the boron-bridged poly(ferrocenylene) **2** with concomitant liberation of diborane(6) (Scheme 1).[12,14,17] In another approach, we have employed the novel ditopic borane 9,10-dihydro-9,10-diboraanthracene $[\mathbf{3}]_n$ for the hydroboration polymerization of aromatic dialkynes, which leads to highly photoluminescent materials.[23−25]

On the basis of these previous investigations, we have now studied the reactivity of 9-H-9-borafluorene (**5**; Figure 1). **5** offers unique opportunities for the preparation of various new classes of boron-doped π-electron materials, because the boron atom is part of a formally antiaromatic central borole ring.[26,27] Consequently, 9-borafluorenes are stronger Lewis acids than acyclic analogs,[28,29] and they are readily reducible to their corresponding dianions.[29−31] These pronounced σ- and π-acceptor properties render 9-borafluorenes highly interesting building blocks for anion sensors and electron-transporting (n-type) materials.[32]

So far, all experimental and theoretical work on the incorporation of 9-borafluorene moieties into larger π-systems has focused on the functionalization of their phenylene rings. A yet unexplored complementary concept would be to use the reactive *B−H bond* in **5** (i) to attach lateral 9-borafluorenyl units to conjugated polymer backbones via the hydroboration of pending alkynyl substituents or (ii) to synthesize well-defined short-chain **4**-type oligomers via the hydroboration of dialkynylarenes. Yet an alternative option is the ring-opening polymerization of **5**, which should lead to 1,1-boranediyl-bridged biphenylenes $[\text{-B(H)-C}_6\text{H}_4\text{-C}_6\text{H}_4\text{-}]_n$. A driving force for such a polymerization sequence should be provided by the loss of antiaromaticity in the monomer. One could envisage substituent scrambling as the underlying reaction mechanism, similar to the reaction leading from **1** to **2** (Scheme 1). In this context we note that the B−C bonds in 9-borafluorene are known to insert BH_3 or BH_2Et under formation of **6**[33] or **7**[34] (Figure 1), respectively, which is precisely the kind of reactivity required for a ring-opening polymerization of **5**.

In this paper, we make use of both, the B−H bond and the B−C bond reactivity of **5**. We will show that this compound can be generated in situ and used immediately for hydroboration

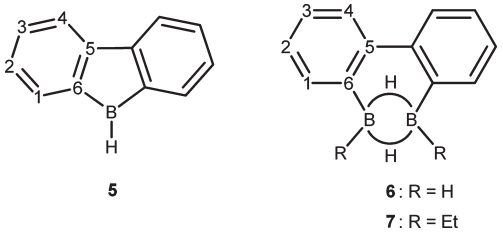

Figure 1. 9-H-9-Borafluorene (**5**) and the insertion products **6** and **7** of BH_3 and BH_2Et into one B−C bond of **5** and 9-Et-9-borafluorene; numbering scheme used for the assignment of NMR resonances.

syntheses. In the absence of a suitable trapping reagent (e.g., a Lewis base or an unsaturated organic molecule), however, **5** undergoes ring-opening polymerization and the corresponding pentamer has been characterized by X-ray crystallography. Moreover, we provide a thorough DFT study on the polymerization mechanism and we elucidate the chain-termination processes both by experimental and by theoretical means.

RESULTS AND DISCUSSION

In situ Generation and a Hydroboration Reaction of 9-H-9-Borafluorene. The parent compound 9-H-9-borafluorene (**5**; Figure 1, Scheme 2) has so far remained elusive and was not available as a hydroboration reagent.[35] However, its pyridine adduct **5·py** as well as lithium 9,9-dihydrido-9-boratafluorene (which can be regarded as the hydride adduct **Li[5·H]**) are literature-known: **5·py** has been prepared by pyrolysis of pyridine-2-biphenylylborane in liquid paraffin at 250 °C,[36] and **Li[5·H]** is accessible from 9-Cl-9-borafluorene and LiH in THF/pentane.[37]

The major reason for the instability of free **5** is most likely a consequence of the 4π antiaromatic nature of the central borole ring, because the propensity to exclude the boron p-orbital from the cyclic conjugation pathway increases the boron Lewis acidity. In contrast to isolable derivatives of **5**, like 9-Ph-9-borafluorene[38,39] or 9-OMe-9-borafluorene,[39] the parent compound is neither stabilized kinetically nor by virtue of a π-donating exocyclic substituent.

9-H,10-H-9,10-dihydro-9,10-diboraanthracene (**3**; Scheme 1) can be prepared in high yields using 9-Br,10-Br-9,10-dihydro-9,10-diboraanthracene and Et_3SiH.[23] The compound is stable under inert conditions even though it contains a formally antiaromatic central ring with an electronic structure comparable to that of the borole ring in 9-H-9-borafluorene (**5**). Given this background, we investigated also the reaction between 9-Br-9-borafluorene (**8**; Scheme 2)[40−42] and Et_3SiH in greater detail.

^1H and $^{13}C\{^1H\}$ NMR spectroscopy on a mixture of **8** and Et_3SiH (C_6D_6, rt) reproducibly revealed a quantitative decrease of the reactant signals and a concomitant appearance of a complex pattern of well-resolved ^1H and ^{13}C resonances which correspond to one single primary product. We note that the conversion rate strongly depends on the absolute concentration and the stoichiometric ratio of the starting materials. If **8** and Et_3SiH are employed in a 1:1 ratio, it takes several hours until the starting material is no longer detectable by NMR spectroscopy; used in a 1:2 ratio, full conversion is achievable within minutes. Since the primary product is subject to a slow follow-up reaction, we found it most convenient to prepare it by the use of 2 equiv of Et_3SiH, because in this case we can reach a stage at which **8** has

dx.doi.org/10.1021/ja110947k |J. Am. Chem. Soc. 2011, 133, 4596–4609

completely vanished while almost no products other than the primary product have formed. This critical point of clean transformation is clearly indicated by a color change from yellow-green to almost colorless.

The $^{11}B\{^1H\}$ NMR spectrum of the primary product shows two broad resonances at 8.5 ppm and 10.3 ppm, testifying to the presence of four-coordinate boron nuclei;[43,44] no multiplets can be resolved upon proton coupling, but the signal at 10.3 ppm becomes significantly broader in the ^{11}B NMR spectrum.

A convincing proposal for the molecular structure of the primary product was possible only after a quantum chemical assessment of the initial stages of the reaction cascade, which allowed us to compute ^1H, ^{11}B, and ^{13}C shift values of all conceivable candidates. Comparison to the experimental data led to the structural assignment presented in the corresponding quantum chemical subsection below. At this point, it suffices to state that (i) the observed NMR signature of Et_3SiBr in the reaction mixture indicates hydride transfer from silicon to boron, (ii) the ^1H and ^{13}C signal pattern is in accord with the formation of a C_1-symmetric dimer $(\mathbf{5})_2$, which does, however, certainly not possess the classical structure $H_8C_{12}B(\mu\text{-}H)_2BC_{12}H_8$ (cf. $[\mathbf{3}]_n$; Scheme 1).

To investigate the reactivity of $(\mathbf{5})_2$, we repeated the transformation between 9-Br-9-borafluorene (**8**) and Et_3SiH in an NMR tube under the same conditions as before (stoichiometric ratio =1:2) and quenched it at the stage of $(\mathbf{5})_2$ with 1 equiv of pyridine (experiment 1) or 0.5 equiv of *tert*-butylacetylene (*t*BuCCH; experiment 2). In both cases, an almost quantitative conversion was finished within minutes. Experiment 1 gave exclusively the known pyridine adduct **5·py**[36] (Scheme 2; see the Supporting Information (SI) for the full NMR data set). Experiment 2 resulted in the formation of the diborylmethane **9** (Scheme 2), together with the monohydroboration product 9-*t*BuC(H)C(H)-9-borafluorene (product ratio =3:1; see the SI for the NMR data and an X-ray crystal structure analysis of 9-*t*BuC(H)C(H)-9-borafluorene).

The constitution of **9**, which we have isolated in analytically pure form in about 50% yield, has been confirmed by an X-ray crystal structure analysis (see below), but is also evident from its NMR spectra: (i) The $^{11}B\{^1H\}$ NMR spectrum shows one broad signal at 71.0 ppm, which lies within the typical shift range of triorganylboranes[44] (cf. 9-Et-9-borafluorene: δ (^{11}B) = 73.1[45]). (ii) The proton integral ratio between the four 9-borafluorene resonances on the one hand and the *tert*-butyl singlet on the other indicates a 2:1 stoichiometry. (iii) We observe a doublet integrating 2H at 2.82 ppm and a triplet integrating 1H at 3.87 ppm; in the HSQC spectrum, the doublet shows a cross peak to a sharp ^{13}C signal at 46.6 ppm while the triplet is associated with a very broad carbon resonance at 36.8 ppm. Since such line broadening is typical for the signals of boron-bonded carbon atoms, the HSQC spectrum leads to the conclusion that both boryl substituents are attached to the same carbon center, which necessarily has to be the terminal one.

The formation of **5·py** and **9** from $(\mathbf{5})_2$ is revealing in several respects: With regard to the general reaction mechanism it becomes evident that $(\mathbf{5})_2$ can readily convert back to **5** in the presence of Lewis bases or C≡C triple bonds. With regard to applications it is pleasing to see that 9-H-9-borafluorene (**5**) can be generated in situ and used efficiently in hydroboration reactions.

Compound **9** not only constitutes important proof for the existence of **5**, but it is also interesting in its own right, because it represents a rigid bifunctional organoborane, in which the two boron atoms are placed in close proximity. Compounds of this kind have found numerous applications,[46] for example as hydride sponges,[47] as cocatalysts in ethylene polymerization,[48] and as catalysts for inverse electron-demand Diels–Alder reactions.[49] In a more exotic context, the intramolecular interaction of the boron p_z-orbitals in 1,8-bis(diphenylboryl)naphthalene has been exploited for the generation of a B–B one-electron σ-bond.[50]

Scheme 2. Synthesis of 5 and Trapping Reactions with Pyridine (py) and *t*BuCCH at Different Points in Time[a]

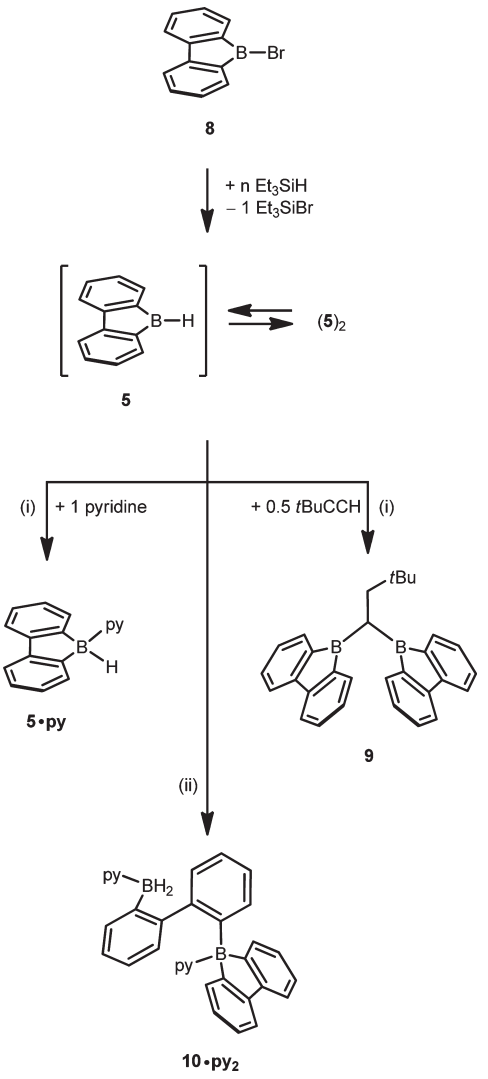

[a] Reagents and conditions: (i) n = 2, C_6H_6, rt, 10–15 min. (ii) 1. n = 1, hexane, rt→5 °C, 7d; 2. precipitate dissolved in C_6H_6, + exc. pyridine, rt.

Crystals of **9** suitable for X-ray analysis were grown from a benzene solution (Figure 2; details of the X-ray crystal structure analysis of **9** are compiled in the SI). As already deduced from the NMR spectra, the compound contains two 9-borafluorenyl moieties per alkyl fragment and both boryl groups are attached to the same carbon atom. All key structural parameters of the 9-borafluorenyl substituents closely resemble those of 9-phenyl-9-borafluorene.[39]

The alkyl bridge of **9** is disordered over two positions (C and C′), which impedes an accurate determination of the B–C(1) bond lengths as well as the B(1)–C(1)–B(2) bond angle (cf.

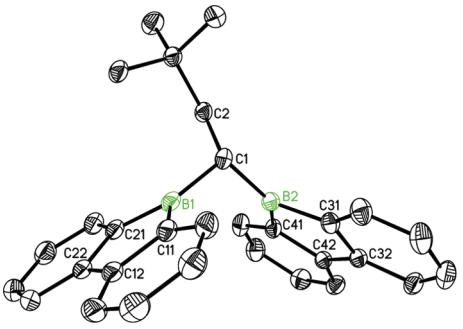

Figure 2. Molecular structure of **9** in the solid state; the minor sites (C′) of the disordered alkyl bridge are not shown (30% probability ellipsoids; H atoms omitted for clarity). Selected bond lengths (Å), atom···atom distance (Å), bond angles (deg), and dihedral angle (deg): B(1)−C(1)/C(1′) 1.586(3)/1.614(7), B(1)−C(11) 1.570(3), B(1)−C(21) 1.585(3), B(2)−C(1)/C(1′) 1.598(2)/1.612(7), B(2)−C(31) 1.569(2), B(2)−C(41) 1.571(2); B(1)···B(2) 2.534(2); C(11)−B(1)−C(21) 103.2(1), C(31)−B(2)−C(41) 103.9(1), B(1)−C(1)/C(1′)−B(2) 105.5(2)/103.5(4); B(1)C(11)C(21)//B(2)C(31)C(41) 74.5.

Figure 2). The most important parameters are the B(1)···B(2) distance of 2.534(2) Å and the dihedral angle of 75° between the two 9-borafluorenyl planes.

Trapping of a Ring-Opened Dimer of 9-H-9-Borafluorene. The reaction mixture of **8** and Et_3SiH in C_6D_6 was monitored by NMR spectroscopy at rt over a period of several days. Thereby, it became obvious that the initial intermediate $(\mathbf{5})_2$ is not long-term stable under these conditions, because the ^1H and ^{13}C NMR spectra gradually changed with time. Noticeably, more and more proton resonances overlapped in the chemical shift interval 6.6 ppm − 7.5 ppm to such an extent that an identification of individual multiplets was no longer possible.

In a series of subsequent experiments, we therefore tried again to trap important constituents of the aged reaction mixtures. We assumed that any higher molecular weight species should be less soluble in aliphatic hydrocarbons than in benzene and therefore switched to hexane as the reaction solvent. We also reduced the reaction temperature to 5 °C to slow down the conversion rate of $(\mathbf{5})_2$. In this way, we obtained a pale yellow precipitate from a hexane solution of **8** and Et_3SiH, which had been stored at 5 °C for 7 d. Since the material was not suitable for single crystal X-ray analysis, we dissolved it at rt in C_6H_6 and treated the solution with excess pyridine. Gas-phase diffusion of hexane into this mixture led to the growth of a few single crystals of the double pyridine adduct $\mathbf{10}\cdot\mathbf{py_2}$ of a 2-biphenylylborane bearing a 9-borafluorenyl substituent (Scheme 2 and Figure 3; details of the X-ray crystal structure analysis of $\mathbf{10}\cdot\mathbf{py_2}$ are compiled in the SI). It is important to note at this stage that the borane $H_2B-C_6H_4-C_6H_4-BC_{12}H_8$ (**10**), which has been trapped in the form of $\mathbf{10}\cdot\mathbf{py_2}$, is *not* identical with $(\mathbf{5})_2$, because the latter compound converts to $\mathbf{5}\cdot\mathbf{py}$ when treated with pyridine.

The B(1)−N(21) = 1.619(4) Å bond length in $\mathbf{10}\cdot\mathbf{py_2}$ agrees with the B−N bond length in the pyridine adduct of 9-Cl-9-borafluorene[51] (average value =1.613(3) Å; two crystallographically independent molecules in the asymmetric unit). The exocyclic bond in $\mathbf{10}\cdot\mathbf{py_2}$ (B(1)−C(31) = 1.632(4) Å) possesses the same length as the two endocyclic bonds (B(1)−C(1) = 1.637(4) Å, B(1)−C(11) = 1.632(4) Å). Most likely as a result of reduced steric congestion, the pyridine ligand as well as the phenyl ring can approach B(2) more closely than in the case of B(1) (cf. B(2)−N(51) = 1.599(4) Å, B(2)−C(42) = 1.617(4) Å).

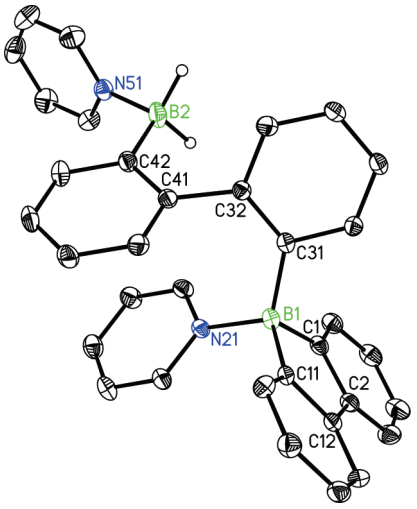

Figure 3. Molecular structure of $\mathbf{10}\cdot\mathbf{py_2}$ in the solid state (30% probability ellipsoids; H atoms on carbon omitted for clarity). Selected bond lengths (Å), bond angles (deg), and dihedral angle (deg): B(1)−N(21) 1.619(4), B(1)−C(1) 1.637(4), B(1)−C(11) 1.632(4), B(1)−C(31) 1.632(4), B(2)−N(51) 1.599(4), B(2)−C(42) 1.617(4); N(21)−B(1)−C(31) 113.1(2), C(1)−B(1)−C(11) 98.9(2), N(51)−B(2)−C(42) 109.5(2); Ar(C(31))//Ar(C(41)) 59.5.

The formation of **10** is reminiscent of the ligand redistribution leading from 1,1′-fc$(B(H)Br)_2$ to the polyferrocenylene [-fc-B(Br)-]$_n$ (**2**) and B_2H_6 (Scheme 1). At the same time, it is a ring-opening process, which lends support to our initial supposition that 9-H-9-borafluorene (**5**) may undergo a ring-opening polymerization to boron-bridged oligophenylenes.

Ring-Opening Oligomerization of 9-H-9-Borafluorene. In the absence of a trapping reagent, storage of a mixture of **8** and Et_3SiH (1:1) in hexane at rt results in the formation of thin yellow crystal plates suitable for X-ray crystallography (details of the X-ray crystal structure analysis are compiled in the SI). Under the conditions specified in the Experimental Section, the first crystals were typically observed after about 7 d, but the crop was usually not harvested earlier than after 1 month. The crystals consist of a remarkable main-chain boron-containing oligophenylene **11** (Figure 4 top), which is a formal ring-opened pentamer (Scheme 3) of 9-H-9-borafluorene (**5**). The molecule bears one BH_2 headgroup (i.e., B(1)) as part of a B_2H_3 terminus and one 9-borafluorenyl end-group (i.e., B(5)). This structural motif is reminiscent of the borane $H_2B-C_6H_4-C_6H_4-BC_{12}H_8$, which we have isolated as pyridine diadduct $\mathbf{10}\cdot\mathbf{py_2}$. All four H-bearing boron atoms, B(1) to B(4), of **11** are engaged in intramolecular B−H−B 3c-2e bonding, thereby establishing two intrastrand cross-links. The tricyclic fragments B(1)-Ar(C(1))-Ar(C(11))-B(2) and B(3)-Ar(C(41))-Ar(C(51))-B(4) closely resemble the literature-known compounds **6** and **7** (Figure 1), which form upon insertion of 0.5 $(H_2BR)_2$ into one endocyclic B−C bond of 9-R-9-borafluorene (*R* = H, Et).[33,34]

The molecular structure of **7** in the solid state has been published.[45] All key metrical parameters of **7** are very similar to those of B(1)-Ar(C(1))-Ar(C(11))-B(2) and B(3)-Ar(C(41))-Ar(C(51))-B(4): The endocyclic $B-C^{Ar}$ bond lengths fall in the interval between 1.548(6) Å (**11**) and 1.582(4) Å (**11**), the

dx.doi.org/10.1021/ja110947k | *J. Am. Chem. Soc.* 2011, 133, 4596–4609

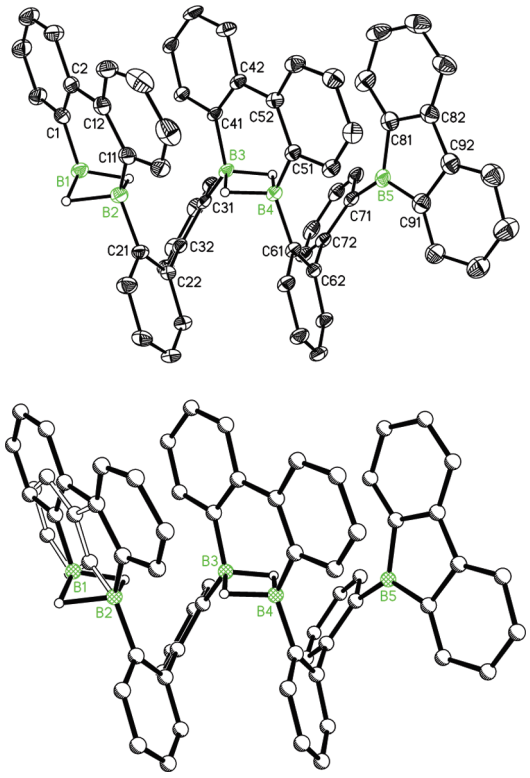

Figure 4. (Top) Molecular structure of **11** in the solid state (30% probability ellipsoids; H atoms on carbon omitted for clarity, one terminal H atom is hidden behind B(1); for schematic views illustrating the boron environments cf. Scheme 3). (Bottom) Superposition of the molecular structures of **11** and **12**, which cocrystallize in the same crystal lattice (stoichiometric ratio: **11**:**12** ≈ 3:1). Selected bond lengths (Å), atom···atom distances (Å), and dihedral angles (deg) of **11**: B(1)−C(1) 1.548(6), B(2)−C(11) 1.570(5), B(2)−C(21) 1.590(4), B(3)−C(31) 1.572(4), B(3)−C(41) 1.582(4), B(4)−C(51) 1.561(4), B(4)−C(61) 1.579(4), B(5)−C(71) 1.571(5), B(5)−C(81) 1.581(5), B(5)−C(91) 1.560(5), B(1)···B(2) 1.806(6), B(3)···B(4) 1.800(4); Ar(C(1))//Ar(C(11)) 7.7, Ar(C(21))//Ar(C(31)) 53.5, Ar(C(41))//Ar(C(51)) 7.0, Ar(C(61))//Ar(C(71)) 53.7, Ar(C(21))//Ar(C(61)) 4.9, Ar(C(31))//Ar(C(71)) 5.1.

B···B distances cover the range between 1.800(4) Å (**11**) and 1.839(4) Å (**7**). Remarkably, **11** cocrystallizes with the closely related oligomer **12** (Scheme 3), which bears *two* 9-borafluorene end-groups (stoichiometric ratio of **11** and **12** in the crystal ≈3:1). A superposition of the two structures is shown in Figure 4 (bottom).

Compound **12** contains five biphenyl moieties, but only four boron atoms. Formally, it can be generated from the pentamer **11** in a chain-termination step by the extrusion of BH_3. We never detected the ^{11}B resonance of B_2H_6 during monitoring NMR studies of the reaction between **8** and Et_3SiH in sealed NMR tubes. However, we take the isolation of compound **13**, which bears two B_2H_3-termini (Scheme 3), as evidence that the extruded BH_3 can be reinserted into the 9-borafluorene tail-group of another molecule of pentamer **11**.

13 crystallizes in very small amounts as yellow blocks that can easily be overlooked in the crop of crystals of **11**/**12** (an X-ray powder diffractogram of the sample containing **11**/**12** and **13** showed an excellent match with the simulated powder diffractogram calculated from the single crystal data of **11**/**12**). A plot of the molecular structure of **13** is presented in Figure 5 (details of the X-ray crystal structure analysis are compiled in the SI). As to be expected, **13** shows similar structural characteristics as **11**, both with regard to the B···B distances and the overall conformation of the oligomer chain.

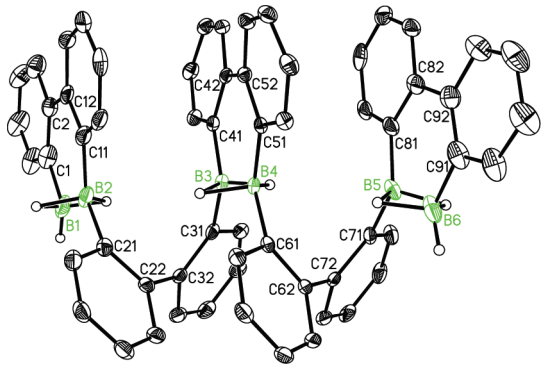

Figure 5. Molecular structure of **13** in the solid state (30% probability ellipsoids; H atoms on carbon omitted for clarity; for a schematic view illustrating the boron environments cf. Scheme 3). Selected bond lengths (Å), atom···atom distances (Å), and dihedral angles (deg): B(1)−C(1) 1.531(8), B(2)−C(11) 1.556(7), B(2)−C(21) 1.578(7), B(3)−C(31) 1.574(6), B(3)−C(41) 1.571(6), B(4)−C(51) 1.569(6), B(4)−C(61) 1.582(6), B(5)−C(71) 1.583(6), B(5)−C(81) 1.548(7), B(6)−C(91) 1.526(8), B(1)···B(2) 1.847(9), B(3)···B(4) 1.792(6), B(5)···B(6) 1.849(9); Ar(C(1))//Ar(C(11)) 1.8, Ar(C(21))//Ar(C(31)) 57.3, Ar(C(41))//Ar(C(51)) 13.6, Ar(C(61))//Ar(C(71)) 56.5, Ar(C(81))//Ar(C(91)) 1.0.

Ring-Opening Dimerization of 9-H-9-Borafluorene. As already outlined above, the ^1H NMR spectrum of a mixture of 9-Br-9-borafluorene (**8**) and Et_3SiH in C_6D_6 first shows the signature of $(\mathbf{5})_2$ and after some time develops an increasingly complex pattern of multiple overlapping resonances, which most likely correspond to higher oligomers. At an even later stage, however, we observed the appearance of two very well-resolved doublets of multiplets exhibiting an unusually strong low-field shift (8.30 ppm, 8.63 ppm). Parallel to that, colorless needle-shaped crystals grew in the NMR tube. Colorless needles were also observed on the surface of the crystal cake of **11**-**13** after prolonged storage of hexane solutions of **8** and Et_3SiH.

An X-ray crystal structure analysis of the needles revealed the cyclic dimer **14** (Scheme 3; Figure 6).[52]

All $B-C^{Ar}$ bond lengths are very close to the corresponding values in **7**;[45] however, the B···B distance in **14** amounts to 1.780(3) Å, compared to a distance of 1.839(4) Å in **7**. Compound **14** adopts a twisted conformation. The dihedral angles between C_6H_4 rings belonging to the same biphenyl unit are 21.1° and 22.4°, while the dihedral angles Ar(C(1))//Ar(C(21)) and Ar(C(11))//Ar(C(31)) are 30.4° and 31.3°, respectively.

Compound **14** is already literature-known and has been synthesized in 15% yield by the reaction of **7** with $BF_3\cdot OEt_2$ (xylene, rt to 130 °C, 4 h).[34] Since these conditions indicate that **14** is a thermodynamically favored molecule, we investigated the reaction between 9-Br-9-borafluorene and Et_3SiH also at elevated temperature (toluene, reflux temperature, 3 h). Already when the mixture was allowed to cool to rt again, crystals of **14** started to grow, and finally we obtained a crystalline yield of 25%. Thus, our synthesis protocol not only provided an authentic sample of **14**, but it also gave access to a compound that has promising potential as building block for two-dimensional

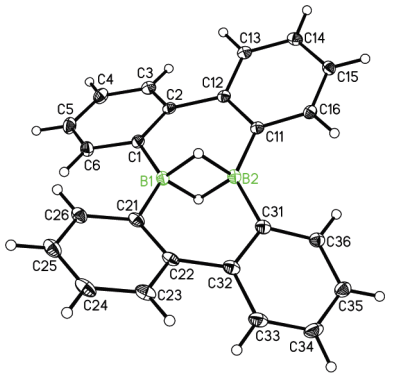

Figure 6. Molecular structure of **14** in the solid state (30% probability ellipsoids). Selected bond lengths (Å), atom···atom distance (Å), bond angles (deg), and dihedral angles (deg): B(1)−C(1) 1.566(3), B(1)−C(21) 1.569(3), B(2)−C(11) 1.570(3), B(2)−C(31) 1.568(3), B(1)···B(2) 1.780(3); C(1)−B(1)−C(21) 132.2(2), C(11)−B(2)−C(31) 131.6(2), B(1)−C(1)−C(2) 120.8(2), B(1)−C(21)−C(22) 120.6(2), B(2)−C(11)−C(12) 120.5(2), B(2)−C(31)−C(32) 120.2(2); Ar(C(1))//Ar(C(11)) 21.1, Ar(C(1))//Ar(C(21)) 30.4, Ar(C(21))//Ar(C(31)) 22.4, Ar(C(11))//Ar(C(31)) 31.3.

boron-doped π-systems. The NMR spectroscopic investigation of **14** confirmed that the signals at 8.30 ppm and 8.63 ppm, which appeared last in the spectrum of the long-term monitoring study (see above), indeed correspond to H-4 and H-1 of the ring-opened cyclic dimer. We therefore conclude that oligomers like **11** (Scheme 3) are the kinetically favored products of the ring-opening reaction of **5**. At elevated temperatures, however, **14** is formed preferentially.

Quantum Chemical Calculations. To provide further insight into the details of the reaction mechanism underlying the experimental observation and to propose a molecular structure for the primary reaction intermediate $(\mathbf{5})_2$, we now turn to the discussion of quantum chemical results.

Dimerization Pathways. Conceptually, the formation of covalently bonded dimers of 9-borafluorene (**A**) can be induced by three independent elementary steps, i.e., *B*−*H*/*B*−*H* (the B−H bond of the first monomer adds across the B−H bond of the second monomer), and the corresponding *B*−*H*/*B*−*C* and *B*−*C*/*B*−*C* addition reactions. We will show in the following that the same three elementary steps are essential also for chain initiation, propagation, and chain termination of higher oligomers.

B−*H*/*B*−*H* reaction between two monomers results in the slightly exoergic formation of the C_{2h}-symmetric diborane **B** with two B−H−B 3c-2e bonds (ΔG_R = −3.3 kcal mol^{-1}; Figure 7). The structural motif of **B** is reminiscent of the unique B−H−B bridged coordination polymer $[\mathbf{3}]_n$ formed by 9,10-dihydro-9,10-diboraanthracene in the crystal lattice.[23] In the 9-borafluorene case, however, we have so far not obtained experimental evidence for the existence of a dimer **B**.

B−*H*/*B*−*C* addition of two monomers leads to intermediate **C** (Figure 8), which features a bridging phenyl ring. The formation of **C** is exoergic but its kinetic stability is limited under the experimental conditions applied: opening of the four-membered BHBC ring is feasible by simultaneous breaking of two juxtaposed bonds, either leading back to **A** with a barrier of 8.7 kcal mol^{-1}, or going forth via $\mathbf{TS_{CD}}$ to **D** with a slightly higher barrier of 11.3 kcal mol^{-1}. **D** contains an intact 9-borafluorene ring and a BH_2 fragment linked by a biphenyl moiety. As we will

Scheme 3. Ring-Opened Pentamer 11 of 5, the Corresponding Oligomers 12 and 13, Which Can Formally Be Generated by Extrusion/Insertion of BH_3 from/into 11, and the Ring-Opened Dimer 14, Which Forms at Elevated Temperatures

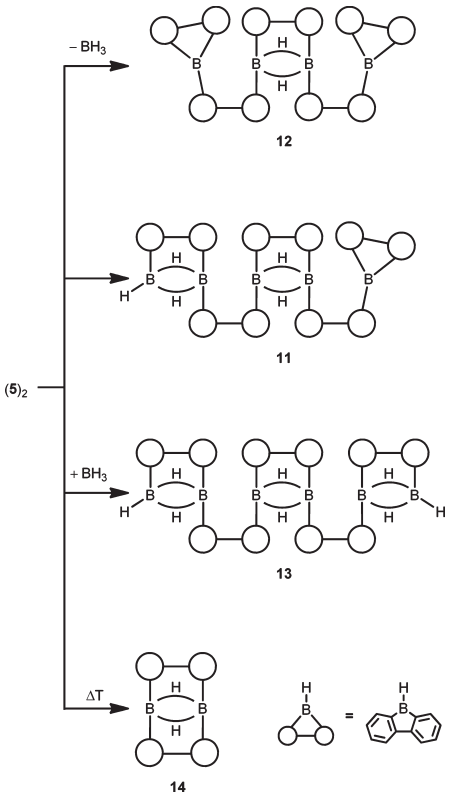

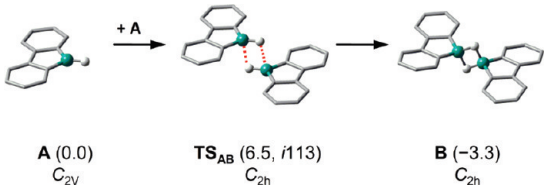

Figure 7. Dimer formation through *B*−*H*/*B*−*H* addition of 9-borafluorene monomers (Gibbs free energies in kcal mol^{-1} relative to two separate molecules of **A**).

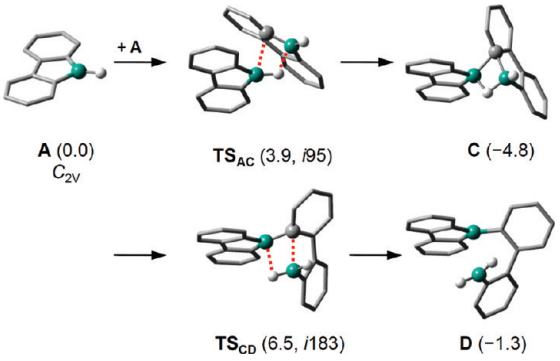

Figure 8. Dimer formation through *B*−*H*/*B*−*C* addition (Gibbs free energies in kcal mol^{-1} relative to two independent molecules of **A**).

dx.doi.org/10.1021/ja110947k |*J. Am. Chem. Soc.* 2011, 133, 4596–4609

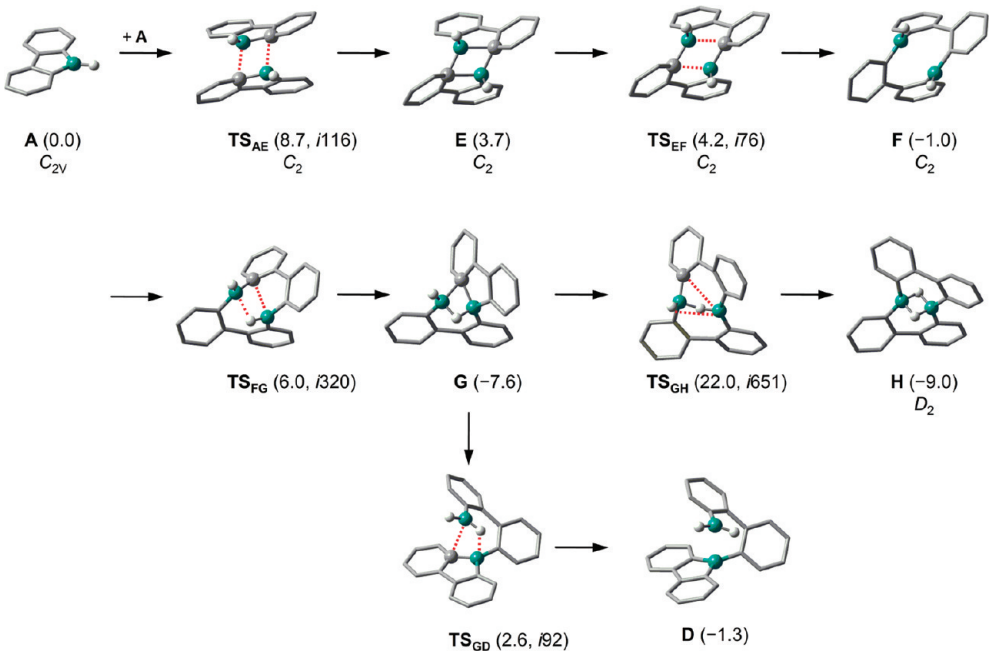

Figure 9. Dimer formation through endo-*B*−*C*/*B*−*C* addition (Gibbs free energies in kcal mol^{-1} relative to two independent molecules of **A**).

illustrate further below, our computed reaction paths indicate that **D** represents a key structure for the build-up of higher 9-borafluorene oligomers for it provides two essential reaction centers, i.e., a primary and a tertiary boron atom. Thus, the experimental proof of the presence of **D** in the reaction mixture (cf. compound **10**·$\mathbf{py_2}$; Scheme 2) is an important validation of this pivotal constituent of the complex overall reaction cascades.

Dimerization through *B*−*C*/*B*−*C* addition can proceed either in an endo- or in an exo-approach of the monomers **A**. The initial barrier of the endo-*B*−*C*/*B*−*C* addition ($\mathbf{TS_{AE}}$, $\Delta G^{\ddagger}$= 8.7 kcal mol^{-1}) is of comparable height to the processes investigated so far. Dimer **E** features *two* boron-bridging phenyl rings (Figure 9). A subsequent, almost barrierless ring-opening step through $\mathbf{TS_{EF}}$ leads to the essentially thermoneutral formation of intermediate **F**. Only a small conformational adjustment is required for an intramolecular *B*−*H*/*B*−*C* addition via $\mathbf{TS_{FG}}$ to yield the phenyl-bridged intermediate **G** with a moderate barrier. Opening of the BHBC ring in **G** via $\mathbf{TS_{GD}}$ provides a second viable path to **D**. In addition, we located $\mathbf{TS_{GH}}$, a transition state which connects **G** with **H**, a particularly interesting product because not only **D** (as pyridine adduct **10**·$\mathbf{py_2}$), but also **H** has been characterized experimentally (cf. **14**; Scheme 3). Yet, although **H** is thermodynamically favored over **D**, the path **G**→$\mathbf{TS_{GH}}$→**H** cannot compete kinetically ($\Delta G^{\ddagger}$ = 29.6 kcal mol^{-1}), and **H** must form via an alternative route.

Indeed, the exo-*B*−*C*/*B*−*C* addition of two monomers **A** provides an energetically favorable pathway to **H** (Figure 10). Both, the first intermediate **I** and the corresponding transition state $\mathbf{TS_{AI}}$, are higher in energy than those of their exo-counterparts **E** and $\mathbf{TS_{AE}}$ due to the lack of stabilizing π−π interactions. However, subsequent ring-opening and a further *B*−*H*/*B*−*H* addition leads in a strongly exoergic final step to **H**. Consequently, with an overall forward barrier of $\Delta G^{\ddagger}$ = 17.4 kcal mol^{-1} and a reaction free energy of ΔG_R = −9.0 kcal mol^{-1} (relative to two monomers **A**) the exo-*B*−*C*/*B*−*C* addition path results in the thermodynamically most favored product identified so far (**H**). With a reverse reaction barrier of $\Delta G^{\ddagger}$ = 22.8 kcal mol^{-1},

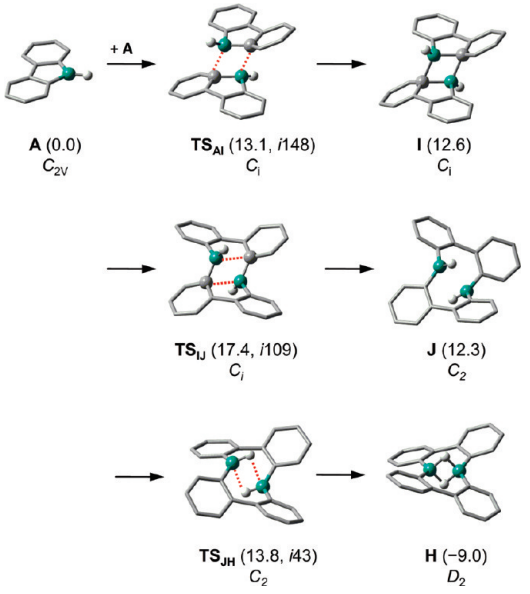

Figure 10. Dimer formation through exo-*B*−*C*/*B*−*C* addition (Gibbs free energies in kcal mol^{-1} relative to two independent molecules of **A**).

H is also kinetically stable. In the sense of a dynamical least-motion principle, all structures constituting this path are already comfortably preorganized for the direct and exclusive formation of the two stable B−H−B bonds present in **H**.

Thus, all reaction sequences along the *B*−*H*/*B*−*H*, the *B*−*H*/*B*−*C*, and the endo-*B*−*C*/*B*−*C* paths involve low barriers and no thermodynamic sinks occur. Only the exo-*B*−*C*/*B*−*C* path yields a well-defined, thermodynamically and kinetically stable product (**H**), provided that sufficient activation energy is available. Under our standard experimental conditions, however, the reversible paths should be dominant and should lead to complex dynamic equilibria. Accordingly, as shown in the NMR experiments, only at very early stages the composition of the reaction

dx.doi.org/10.1021/ja110947k |*J. Am. Chem. Soc.* 2011, 133, 4596–4609

mixture is dominated by one single species $(\mathbf{5})_2$. A comparison of relative free energies of the intermediates along the reaction pathways studied so far renders **B**, **C**, and **G** relevant candidates to assign a structure to $(\mathbf{5})_2$.

The experimental ^{1}H NMR spectrum of the primary product $(\mathbf{5})_2$ is characterized by eight doublets and eight virtual triplets/doublets of doublets, all possessing the same integral value (neglecting $^4J_{HH}$ coupling in this description). The experimental $^{13}C\{^1H\}$ NMR spectrum contains 16 *C*H resonances together with eight signals assignable to quaternary carbon nuclei, four of which show the extreme signal broadening typical[43] of boron-bonded carbon atoms. Hence, at this point, we can already exclude **B** because of its high symmetry.

The two remaining structures (**C** and **G**; Figure 11), however, possess C_1 symmetry and thus four magnetically inequivalent C_6H_4 rings I−IV. In line with that, all experimentally observed ^{1}H and ^{13}C signals can be assigned to four different C_6H_4 rings with the help of H,H COSY and HSQC experiments; a HMBC experiment revealed that rings I and II as well as III and IV are tied together to form two *o*,*o*′-diborylated biphenyl fragments. We note that the ^{1}H chemical shift values of I to IV are spread over the wide range between 6.14 ppm and 8.40 ppm, but that the proton signals of the biphenyl unit I−II have rather similar chemical shifts. The ^{13}C chemical shifts of corresponding *C*H and C-5 (cf. Figure 1) nuclei in rings I to III fall within the narrow range of ±5 ppm. In contrast, ring IV is characterized by several abnormal NMR features: (i) one *C*H atom resonates at 151.6 ppm, which is 15−30 ppm downfield from all other *C*H signals; (ii) the chemical shift value of the C-5 nucleus is 169.6 ppm, as opposed to 140.9, 142.0, and 145.0 ppm for rings I to III; (iii) the chemical shift value of the C-6 (cf. Figure 1) nucleus is 114.2 ppm, which has to be compared to values of 137.4, 139.1, and 149.7 ppm for rings I−III (see the SI for a plot of selected NMR spectra and a detailed compilation of all chemical shift values).

Computed ^{1}H and ^{13}C NMR shifts of **C** and **G** show a significantly better match of experimental and computed data for the latter (the SI contains a full presentation of data, including a calibration for the NMR computations). Figure 11 shows the most revealing features of **C** and **G**. For both species the unusual ^{13}C resonances (see above) can be attributed to the boron-bridging phenyl rings. However, we can discriminate between **C** and **G** using the ^{11}B shift values, as well as the ^{13}C NMR data for C-5 (cf. Figure 1) and the corresponding ^{1}H signals of the ortho protons of rings I and II. In line with investigations of Wrackmeyer,[45] fragments of type **5** show C-5 shift values around 150 ppm, whereas in fragments of type **6** the C-5 resonances appear around 140 ppm. Also, the ortho ^{1}H resonances appear around 7.5 ppm in the former case, but around 8.5 ppm in the latter. While $(\mathbf{5})_2$ reacts as a direct source of **5** (as shown in the trapping experiments), the NMR spectroscopic evidence indicates that it is structurally more closely related to the ring-opened compound **6** (Figure 1). The NMR calculations on **G** reproduce all experimental chemical shift values of $(\mathbf{5})_2$ with a mean signed deviation of 0.14 ± 0.17 ppm (^{1}H), −0.6 ± 1.9 ppm (^{13}C), or −1.1 ± 1.1 ppm (^{11}B), and we feel safe to propose the identity of $(\mathbf{5})_2$ and **G**.[53,54]

So far, we conclude that our quantum chemical predictions are fully in line with our most compelling experimental observations: (i) neither 9-H-9-borafluorene **A** (= **5**) nor its B−H−B-bridged dimer **B** are detectable by in situ NMR spectroscopy; instead, we observe clearly distinct signatures of a dimer $(\mathbf{5})_2$, and we identify

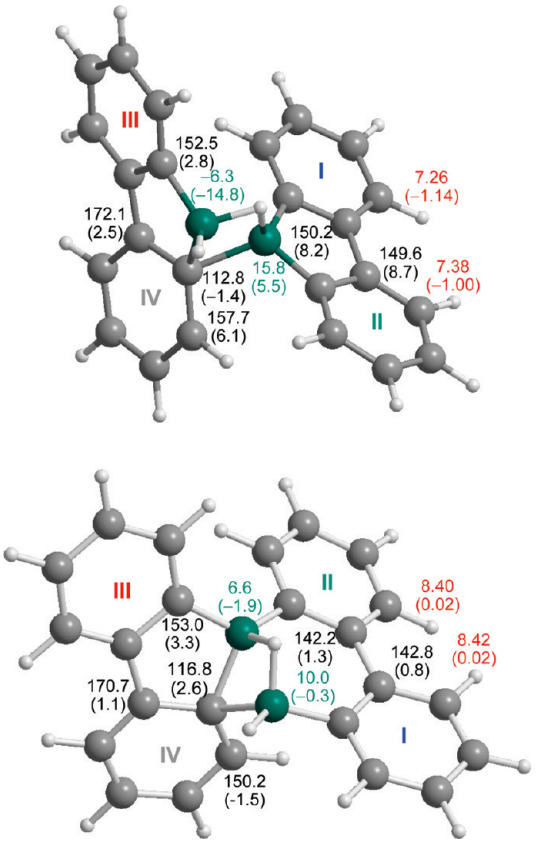

Figure 11. Selected computed ^{1}H (red), ^{13}C (black), and ^{11}B (green) NMR chemical shift values for **C** (top) and **G** (bottom; B97D/TZVP GIAO calculations, deviations from experiment given in parentheses).

this compound as the phenyl-bridged species **G**. (ii) At room temperature, a mixture of 9-Br-9-borafluorene (**8**) and Et_3SiH in C_6D_6 has to be kept for weeks before the NMR signature of **H** (= **14**) occurs; from refluxing toluene, however, **14** precipitates in yields of 25% within a few hours. (iii) **D** obviously exists in the aged reaction mixture and can be isolated in relevant amounts by trapping with pyridine (cf. $\mathbf{10}\cdot\mathbf{py_2}$).

Against this background, we investigated the fate of **D** in more detail, focusing first on its BH_2 headgroup for its obvious inherent reactivity.

Reactivity of the BH_2 Headgroup in D. Relevant reaction partners of **D** include added Lewis bases such as pyridine as well as 9-H-9-borafluorene **A**. Dimerization of **D** is not considered given the supposedly low stationary concentration of this highly reactive species under the experimental conditions applied.

In line with the successful isolation of the pyridine adduct $\mathbf{10}\cdot\mathbf{py_2}$, we computed the B−N binding energies of $\mathbf{D}\cdot\mathbf{py}$ and $\mathbf{D}\cdot\mathbf{py_2}$ (which corresponds to $\mathbf{10}\cdot\mathbf{py_2}$) and found a significant thermodynamic driving force of $\Delta G_R = -23.1$ kcal mol^{-1} toward the formation of $\mathbf{D}\cdot\mathbf{py_2}$. In comparison, the formation of the pyridine adduct $\mathbf{A}\cdot\mathbf{py}$ (= $\mathbf{5}\cdot\mathbf{py}$; Scheme 2) is thermodynamically less favored ($\Delta G_R = -15.0$ kcal mol^{-1}; cf. SI).

As illustrated in Figure 12, **K** is readily formed from **A** and **D** via *B*−*H*/*B*−*H* addition. Although this step represents a headgroup protection of **D**, we will demonstrate below that **K** still is an important starting point of further reaction cascades.

Alternatively, **D** can also act as a hydride donor for a monomer **A** through *B*−*H*/*B*−*C* addition. Figure 13 compiles the subsequent, surprisingly facile reaction cascade to **N**, which proceeds

dx.doi.org/10.1021/ja110947k | *J. Am. Chem. Soc.* 2011, 133, 4596–4609

exclusively via the elementary steps already introduced above. Trimer **N** is formed with a moderate overall barrier of $\Delta G^{\ddagger} = 7.7$ kcal mol^{-1} and constitutes (apart from the pyridine diadduct **D**·**py**$_2$) the thermodynamically most favorable species encountered so far ($\Delta G_R = -19.8$ kcal mol^{-1} with respect to **D** plus **A**; $\Delta G_R = -21.1$ kcal mol^{-1} with respect to three independent units of **A**). We note that **N** already features all relevant structural characteristics of compound **11** (Figure 4), the major constituent of the crystalline precipitate, i.e., a 9-phenyl-9-borafluorene tail-group, a biphenylene linker, and a biphenylene-bridged B_2H_3 moiety.

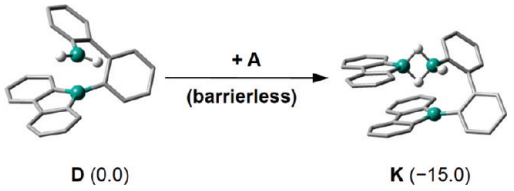

Figure 12. Protection reaction of the BH_2 headgroup of **D** with **A** (Gibbs free energies in kcal mol^{-1} relative to separated **D** plus **A**).

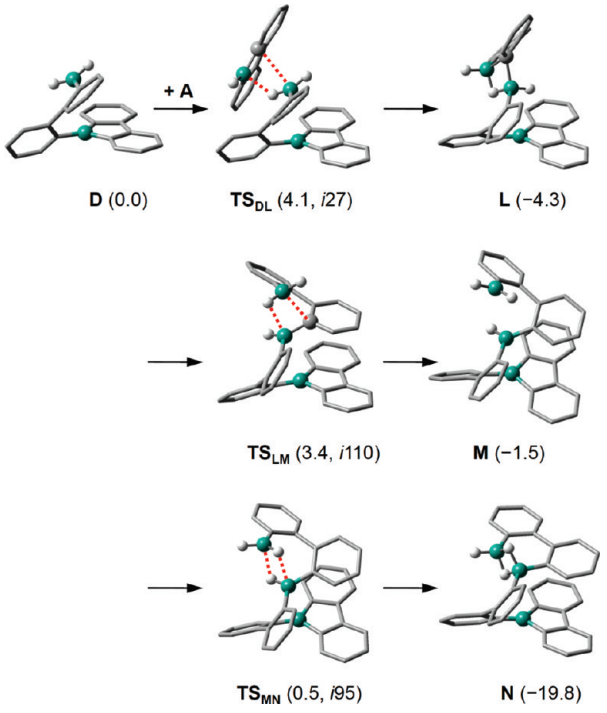

Figure 13. *B*−*H*/*B*−*C* addition of the BH_2 headgroup of **D** to **A** (Gibbs free energies in kcal mol^{-1} relative to separated **D** plus **A**).

Reactivity of the 9-Borafluorenyl Tail-Group in K. *B*−*H*/*B*−*C* addition of a monomer **A** to **K** can occur across all three bonds about the tertiary boron atom in the 9-borafluorene tail-group. B−H addition across the exocyclic B−C bond constitutes an unproductive identity reaction. *B*−*H*/*B*−*C* addition across either of the two endocyclic B−C bonds leads to chain propagation; however, the inherent chirality of a biphenyl bridge renders the two B−C bonds inequivalent. We explicitly studied both paths using the unprotected dimer **D** as a model system (see the SI for details). Since both reaction sequences do not exhibit any appreciable kinetic or thermodynamic differences, we only investigated the energetically (slightly) favorable chain propagation steps for the more realistic intermediate **K** (Figure 14). The reaction cascade involves the usual elementary steps with an overall barrier of $\Delta G^{\ddagger} = 13.9$ kcal mol^{-1} and first leads to **P**, which contains a valence-unsaturated central diorganyl borane group. Subsequent rotation of this group about two B−C bonds results in a conformation from which two intramolecular B−H−B bonds are established in a concerted process with concomitant extrusion of the protective group **A**. Most notably, the final species resulting from this sequence is identical to the product **N** formed by the *B*−*H*/*B*−*C* attack of the BH_2 headgroup of **D** on a monomer **A** discussed above (Figure 13). **N** represents the smallest oligomer of an entire series, comprising also the experimentally characterized species **11** (Figure 4). We therefore focus in the following section on chain propagation processes commencing with **N**.

Chain Propagation. In principle, the transition from **K** to **N** is just an isomerization reaction and its driving force is provided by the loss of antiaromaticity resulting from the (formal) ring expansion of the BH_2-protecting 9-H-9-borafluorene moiety. It is therefore not surprising that the reactivity of the 9-borafluorenyl tail-groups toward an incoming monomer **A** is essentially the same in **K** and **N** (cf. Figures 14 and 15). With **R** (Figure 15), we encounter an intermediate that bears close

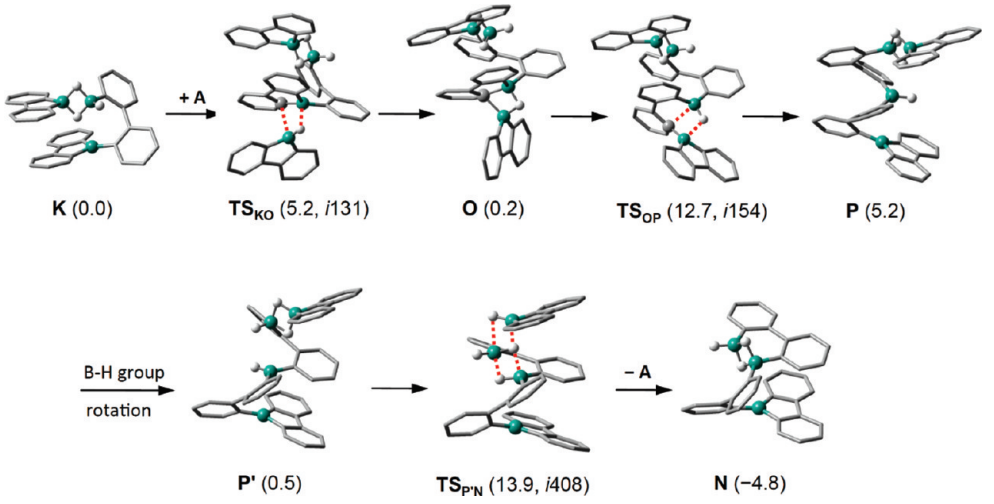

Figure 14. *B*−*H*/*B*−*C* addition of **A** to the tail-group of **K** (Gibbs free energies in kcal mol^{-1} relative to **K**).

dx.doi.org/10.1021/ja110947k | *J. Am. Chem. Soc.* 2011, 133, 4596–4609

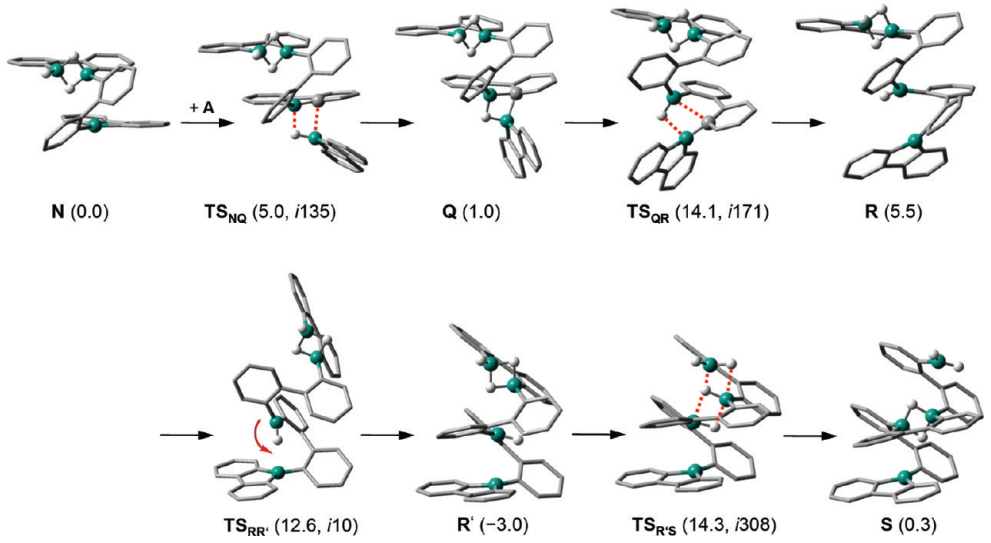

Figure 15. *B*−*H*/*B*−*C* addition of **A** to the tail-group of **N** (Gibbs free energies in kcal mol^{-1} relative to **N** plus **A**).

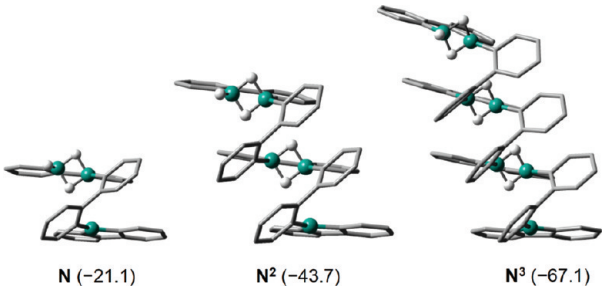

Figure 16. Oligomers **N**, **N**^{2}, and **N**^{3} (Gibbs free energies in kcal mol^{-1} relative to the equivalent number of independent **A**).

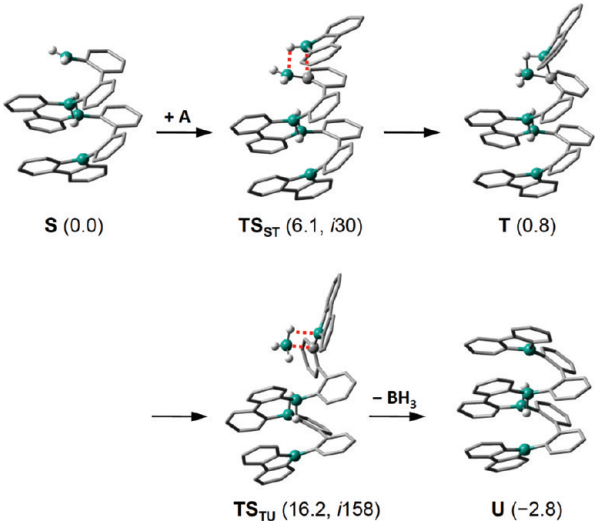

Figure 17. Chain termination by *B*−*H*/*B*−*C* addition of **A** to the BH_2 headgroup of **S** and subsequent elimination of BH_3 (Gibbs free energies in kcal mol^{-1} relative to **S** plus **A**).

resemblance to **P** (Figure 14), and it is again the unsaturated nature of this species that governs the course of the subsequent reactions.

As before, internal B−C rotation (**TS**$_{RR'}$) orients the dangling B−H bond such that the unsaturated active boron site is shifted from its internal position (**R**/**R**′) to the periphery of the molecule (**S**) in a concerted process. This shift generates a primary BH_2 headgroup and thus substantially enhances the disposition of the molecule for further intermolecular reactivity. **S** differs from **D** only by the presence of an (innocent) internal spacer between the two crucial functional groups, i.e., a BH_2 head and a 9-borafluorenyl tail. The fate of **S** is readily deducible from the reactivity patterns identified for **D**: both the headgroup reactivity and the tail-group reactivity established before (Figure 13 and Figure 14, respectively) will lead to the same **N**-type product (**N**^{2}; Figure 16), but now augmented by the first repeat unit of a growing polymer chain. Because of the obvious structural and energetic incremental behavior of the elementary steps involved, we refrained from explicit calculations of the reaction pathway.

Our mechanistic proposal finds strong support by the successful experimental characterization of **N**^{2} (= **11**; Figure 4). However, the list of potential reaction partners is obviously more complex than explicitly considered above, e.g., headgroup attack of **D** to the tail-group of **N** represents a short cut to the higher oligomer **N**^{2} (Figure 16). Yet, for a comprehensive description of the general picture it suffices to focus on the few key elementary steps involved, rather than on the wealth of possible reaction partners.

It remains to be elucidated whether thermodynamics pose a natural limit to chain propagation. Figure 16 compiles the computed structures along the sequence of oligomers from **N** to **N**^{3} and the relative free energies with respect to the corresponding numbers of free monomers **A**. We conclude that already for low-molecular-weight oligomers the two chain ends behave essentially as independent fragments and every repeating unit added contributes an increment of about $\Delta G_{inc} = -23$ kcal mol^{-1} to the thermodynamic stability of the resulting polymer.

Chain Termination. In this section we exclusively consider the two species that have been characterized experimentally, i.e., **12** and **13** (Figures 4 and 5). Straightforward access would formally involve BH_3 elimination from **11** (= **N**^{2}) and subsequent insertion into the 9-borafluorenyl tail-group of another molecule of **11**. While we did not identify any energetically

dx.doi.org/10.1021/ja110947k | *J. Am. Chem. Soc.* 2011, 133, 4596–4609

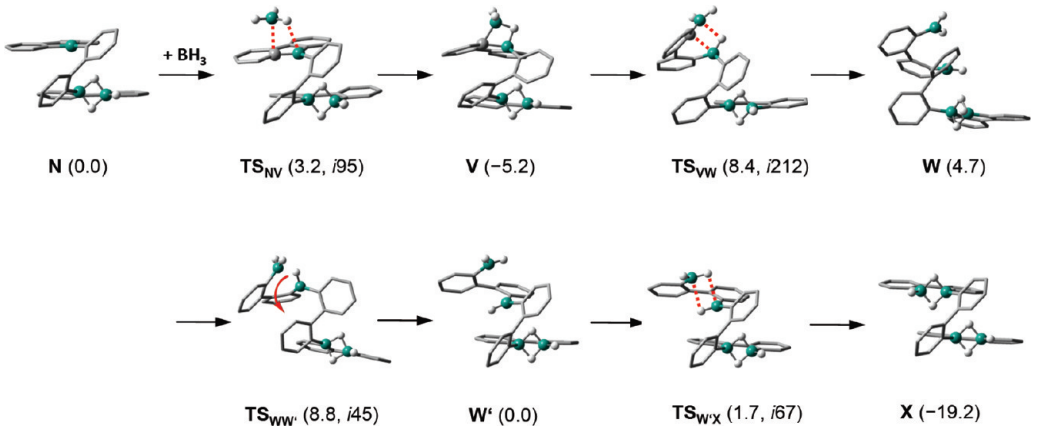

Figure 18. Chain termination by *B*−*H*/*B*−*H* addition of BH_3 to the tail-group of **N** (Gibbs free energies in kcal mol^{-1} relative to **N** plus BH_3).

feasible direct process for BH_3 extrusion from $\mathbf{N}^2$, we found that species like **S** represent bifurcation points either for chain propagation (e.g., $\mathbf{S}+\mathbf{A}\rightarrow\mathbf{N}^2$ = **11**) or chain termination ($\mathbf{S}+\mathbf{A}\rightarrow\mathbf{U}$ = **12**; Figure 17): *B*−*H*/*B*−*C* addition of **A** to the BH_2 headgroup of **S** yields intermediate **T** and subsequent BH_3 elimination generates **U**.

The insertion of BH_3 into an endocyclic B−C bond of the 9-borafluorene tail-group in $\mathbf{N}^2$ is indeed a viable process to form oligomers **13**, carrying two B_2H_3 termini. We studied the corresponding reaction pathway for the smallest relevant model system **N** (Figure 18). The highly exoergic reaction $\mathbf{N}+BH_3\rightarrow\mathbf{X}$ (ΔG_R = −19.2 kcal mol^{-1}) commences with an almost barrierless *B*−*H*/*B*−*C* BH_3 addition step, followed by a rate-limiting ring-opening via $\mathbf{TS_{VW}}$ ($\Delta G^{\ddagger}$ = 13.6 kcal mol^{-1}), concerted rotations about internal B−C and C−C bonds, and a subsequent almost barrierless intramolecular *B*−*H*/*B*−*H* addition. Compared to the series **N** to $\mathbf{N}^3$ (Figure 16), we find the same incremental behavior (ΔG_{inc} = −23 kcal mol^{-1}) of the relative free energies along the series of corresponding products of this chain termination step, **X** to $\mathbf{X}^3$(cf. SI). The computed moderate barrier for this reaction sequence ($\Delta G^{\ddagger}$ = 13.6 kcal mol^{-1} with respect to **N**) is fully in line with the fact that we did not observe any free B_2H_6 in our monitoring NMR studies described above.

CONCLUSION

9-H-9-Borafluorene ($H_8C_{12}BH$, **5**), which can easily be generated by Br/H exchange between 9-Br-9-borafluorene and Et_3SiH, is a versatile reagent for the preparation of boron-doped π-conjugated materials. We have shown that (i) it readily hydroborates *tert*-butylacetylene but also that (ii) in the absence of a trapping reagent it undergoes a ring-opening polymerization reaction leading to B(H)-bridged biphenylenes $H[-(H)B-(C_6H_4)_2-]_nBC_{12}H_8$. The corresponding pentamer **11** (n = 4) has been characterized in the solid state by X-ray crystallography; the compound shows two intrastrand B−$(\mu$-H$)_2$−B cross-links.

The reaction mechanism underlying polymer formation has been elucidated in a joint experimental and theoretical study. Three elementary steps, i.e., addition of a B−H bond across another B−H bond, B−H/B−C addition, and B−C/B−C addition, are sufficient to explain chain initiation, chain propagation as well as chain termination. In situ NMR spectroscopy on solutions of 9-Br-9-borafluorene and Et_3SiH (C_6D_6, rt) revealed signals assignable to a C_1-symmetric dimer $(\mathbf{5})_2$ as primary reaction intermediate. Computed ^1H, ^{13}C, and ^{11}B chemical shift values of various conceivable isomers of $(\mathbf{5})_2$ gave an excellent match for a structure featuring one B−H−B 3c-2e bond and one boron-bridging phenyl ring. This species then ring-opens to give the borane $H_2B-C_6H_4-C_6H_4-BC_{12}H_8$ (**10**). **10** can react with a monomer **5** either via the BH_2 headgroup or via the 9-borafluorenyl tail-group. In both cases, the final products are identical, i.e., the trimer $H[-(H)B-(C_6H_4)_2-]_2BC_{12}H_8$, which stabilizes itself by two intramolecular B−H−B 3c-2e bonds and is a shorter congener of oligomer **11**. Further chain growth can readily proceed via (i) B−H attack of a monomer **5** on an endocyclic B−C bond of oligomers $H[-(H)B-(C_6H_4)_2-]_n$-$BC_{12}H_8$ if n is an even number, or (ii) B−C attack of a monomer **5** on the free BH_2 headgroup of $H[-(H)B-(C_6H_4)_2-]_nBC_{12}H_8$ if n is an odd number. Chain termination occurs by BH_3 extrusion during BH_2 headgroup attack of **A** and gives oligomers $H_8C_{12}B-(C_6H_4)_2[-(H)B-(C_6H_4)_2-]_nBC_{12}H_8$ bearing two 9-borafluorenyl termini (cf. the crystallographically characterized compound **12**; n = 2). Alternatively, BH_3 can insert into the 9-borafluorenyl tail groups of growing polymer chains, thereby generating a $H[-(H)B-(C_6H_4)_2-]_nBH_2$ species (cf. the crystallographically characterized compound **13**; n = 5). At our present stage of knowledge we have to assume that in the case of **11** the chain length is mainly determined by the low solubility of the compound in hexane, because theory has established that there is no obvious thermodynamic limit to chain growth. We are presently evaluating possibilities to prepare higher oligomers or even polymers by introduction of solubilizing side chains.

Our results indicate that it should be possible to transform a mixture of, e.g., **11**, **12**, and **13** into pure **13** by treatment with B_2H_6. Moreover, hydroboration of alkynes with such oligomers should lead to corresponding oligophenylenes $[-(R)B-(C_6H_4)_2-]_n$ with three-coordinate boron bridges, for which we expect highly interesting optoelectronic properties.

Finally, we note that intrastrand B−$(\mu$-H$)_2$−B cross-links as in **11**, **12**, and **13** offer new ways to modulate the conformational flexibility as well as the electronic structure of such macromolecules by, for example, temperature increase to thermally open the B−H−B bonds.

EXPERIMENTAL METHODS

General Remarks. All reactions were carried out under a nitrogen atmosphere using Schlenk tube techniques or in an argon-filled glovebox. Reaction solvents were either freshly distilled under argon from Na/

dx.doi.org/10.1021/ja110947k |*J. Am. Chem. Soc.* 2011, 133, 4596–4609

Pb alloy (alkanes) and Na/benzophenone (benzene, toluene, C_6D_6) or dried over molecular sieves (4 Å; $CDCl_3$) prior to use. NMR: Bruker Avance 300, Avance 400, and Avance 600. Chemical shifts are referenced to (residual) solvent signals (^1H, $^{13}C\{^1H\}$) or external $BF_3 \cdot OEt_2$ ($^{11}B\{^1H\}$). Abbreviations: s = singlet, d = doublet, t = triplet, vt = virtual triplet, m = multiplet, br = broad, n.o. = signal not observed. **8** was synthesized following a literature procedure.[42]

Synthesis of 9. Neat Et_3SiH (390 μL, 285 mg, 2.45 mmol) was added via syringe at rt to a slowly stirred solution of **8** (311 mg, 1.28 mmol) in C_6H_6 (5.5 mL). After approximately 10 min, the color of the mixture changed from yellow-green to almost colorless. This point corresponds to the quantitative consumption of **8** with formation of $(\mathbf{5})_2$ (NMR spectroscopic control). Neat *t*BuCCH (90 mL, 60 mg, 0.73 mmol) was added via syringe and stirring was continued at rt for 15 min, whereupon the color of the solution changed to an intense yellow; a slight heat development was noticeable. The mixture was stored at 5 °C in a refrigerator for 1 h, whereupon a yellow microcrystalline solid precipitated. The mother liquor was removed via syringe, and the solid product, which turned out to be analytically pure **9**, was dried under dynamic vacuum. Yield: 124 mg (0.30 mmol; 47%). Single cystals of **9** were grown by recrystallization from C_6H_6.

All volatiles were removed from the mother liquor under dynamic vacuum to yield a yellow oily residue. After approximately 12 h, part of the oily residue had transformed into yellow crystals, which turned out to be a second crop of **9** (NMR spectroscopic control). A close inspection of the crystalline material revealed the presence of very few yellow-green needles that consisted of the monohydroboration product 9-*t*BuC(H)C(H)-9-borafluorene. According to ^1H NMR spectroscopy, the ratio of **9** and 9-*t*BuC(H)C(H)-9-borafluorene in the oily residue was 1:1; we found no evidence for the presence of significant amounts of other products (see the SI for NMR data and an X-ray crystal structure analysis of 9-*t*BuC(H)C(H)-9-borafluorene).

^1H NMR (400.1 MHz, C_6D_6): δ 0.93 (s, 9H; CH_3), 2.82 (d, $^3J_{HH}$ = 6.7 Hz, 2H; CH_2), 3.87 (t, $^3J_{HH}$ = 6.7 Hz, 1H; C*H*CH_2), 6.88 (vtd, $^4J_{HH}$ = 1.3 Hz, 4H; H-2), 6.95 (vtd, $^4J_{HH}$ = 1.3 Hz, 4H; H-3), 6.99 (m, 4H; H-4), 7.92 (dm, $^3J_{HH}$ = 6.9 Hz, 4H; H-1). $^{11}B\{^1H\}$ NMR (96.3 MHz, C_6D_6): δ 71.0 (br). $^{13}C\{^1H\}$ NMR (75.4 MHz, C_6D_6): δ 29.7 (CH_3), 32.6 (CCH_3), 36.8 (br, $CHCH_2$), 46.6 (CH_2), 119.8 (C-4), 128.4 (C-2), 134.2 (C-3), 134.6 (C-1), 142.7 (br, C-6), 153.8 (C-5). Elemental analysis calcd (%) for $C_{30}H_{28}B_2$ (410.14): C 87.86, H 6.88; found: C 87.65, H 6.90.

Synthesis of $\mathbf{10 \cdot py_2}$. A stirred solution of **8** (160 mg, 0.66 mmol) in hexane (17 mL) was treated at rt with neat Et_3SiH (130 μL, 95 mg, 0.82 mmol). The mixture was stored at 5 °C in a refrigerator for 7 d, whereupon a pale-yellow microcrystalline precipitate formed. The mother liquor was removed via syringe. The solid residue was dried in vacuo, dissolved in C_6H_6 (5 mL), and treated with an excess of neat pyridine (0.40 mL, 390 mg, 5.00 mmol). After 0.5 h stirring at rt, the clear, pale-red solution was evaporated to dryness in vacuo in order to remove unreacted pyridine. The resulting solid residue was redissolved in C_6H_6 (3 mL). Single crystals of $\mathbf{10 \cdot py_2}$ suitable for X-ray analysis were obtained by gas-phase diffusion of hexane into this solution.

Synthesis of 11, 12, and 13. Neat Et_3SiH (200 μL, 146 mg, 1.26 mmol) was added via syringe at rt to an ampule containing a solution of **8** (271 mg, 1.12 mmol) in hexane (30 mL). The ampule was cooled to liquid-nitrogen temperature, vacuum sealed, and allowed to warm to rt. From the clear, yellow solution obtained, crystals grew over a period of approximately 1 month. The ampule was opened in a glovebox, and the mother liquor was removed from the crystalline material using a syringe. The crystal crop was carefully examined with a microscope to determine its homogeneity. The vast majority of crystals turned out to be thin yellow platelets (i.e., **11**/**12**), which were accompanied by very few yellow crystals of slightly different habit (i.e., **13**) and some colorless needles (i.e., **14**). An X-ray powder diffractogram of the crystal mixture turned out to be a superposition of the powder diffractograms calculated from the single-crystal data of **11**/**12** and **14**; **11**/**12** were by far the dominating species, and the signature of **13** could not be detected at all.

We note that crystallization of **11**−**14** is a continuous process. After one month, an overall yield of about 20% (with respect to **8**) can be harvested; if the ampule is stored for 3−4 months, the oligomer yield reproducibly exceeds 50%.

The colorless needles of **14** were manually removed from the sample used for the elemental analysis. Elemental analysis calcd (%) for 0.75 $C_{60}H_{45}B_5$ × 0.25 $C_{60}H_{42}B_4$ × 0.5 C_6H_{14} (859.64): C 88.02, H 6.01; found: C 87.88, H 5.76.

Synthesis of 14. A stirred solution of **8** (336 mg, 1.38 mmol) in toluene (20 mL) was heated to reflux temperature. A solution of Et_3SiH (350 μL, 255 mg, 2.19 mmol) in toluene (20 mL) was added dropwise over a period of 1 h. After the addition was complete, heating was continued for another 2 h. The clear yellow solution obtained was allowed to cool to rt, whereupon thin colorless needles formed. The mixture was stored at rt for 16 h, the mother liquor was removed using a syringe, and the crystal crop was dried under vacuum. Yield: 56 mg (0.17 mmol; 25%). X-ray-quality crystals were obtained by recrystallization from C_6H_6.

^1H NMR (400.1 MHz, C_6D_6): δ 3.12 (br, 2H; BH), 7.38 (vtd, $^4J_{HH}$ = 1.2 Hz, 4H; H-2), 7.48 (vtd, $^4J_{HH}$ = 1.5 Hz, 4H; H-3), 8.30 (dm, $^3J_{HH}$ = 8.2 Hz, 4H; H-4), 8.63 (dd, $^3J_{HH}$ = 7.5 Hz, $^4J_{HH}$ = 1.5 Hz, 4H; H-1). ^1H NMR (300.0 MHz, $CDCl_3$): δ 7.59 (vtd, $^4J_{HH}$ = 1.2 Hz, 4H; H-2), 7.70 (ddd, $^3J_{HH}$ = 8.1, 8.2 Hz, $^4J_{HH}$ = 1.6 Hz, 4H; H-3), 8.52 (dm, $^3J_{HH}$ = 8.2 Hz, 4H; H-4), 8.76 (dd, $^3J_{HH}$ = 7.6 Hz, $^4J_{HH}$ = 1.6 Hz, 4H; H-1). $^{11}B\{^1H\}$ NMR (96.3 MHz, $CDCl_3$): δ 11.0 ($h_{1/2}$ = 300 Hz). $^{13}C\{^1H\}$ NMR (75.4 MHz, $CDCl_3$): δ 126.8 (C-2), 127.6 (C-4), 129.8 (C-3), 132.9 (C-1), 142.6 (C-5), n.o. (C-6).

Crystal Structure Analyses. Crystals of **9**, 9-*t*BuC(H)C(H)-9-borafluorene, and $\mathbf{10 \cdot py_2}$ were measured on a STOE IPDS-II diffractometer with graphite-monochromated Mo Kα radiation. Crystals of **11**/**12**, **13**, and **14** were measured on a Bruker CCD three-circle diffractometer equipped with an INCOATEC microsource generator with multilayer optics. The structures were solved by direct methods using the program SHELXS[55] and refined with full-matrix least-squares on F^2 using the program SHELXL97.[56] Hydrogen atoms bonded to C were placed on ideal positions and refined with fixed isotropic displacement parameters using a riding model. In $\mathbf{10 \cdot py_2}$ the H atoms bonded to B were found in a difference map and were freely refined. The H atoms bonded to B in **11**/**12** were found in a difference map; the fully occupied ones were freely refined, the partially occupied ones were refined using a riding model. The H atoms bonded to B in **13** were found in a difference map; the coordinates of six of the eight H atoms were refined, whereas the remaining two were refined using a riding model. In **14**, the H atoms bonded to B were found in a difference map and were freely refined.

In **9**, the neohexyl residue is disordered over two positions. The site occupation factor of the major occupied sites is 0.748(4). The minor occupied atoms were isotropically refined. Similarity restraints were used for the two different sites.

9-*t*BuC(H)C(H)-9-borafluorene formed nonmerohedrally twinned crystals. The fractional contribution of the major domain was 0.655(5). Hydrogen atoms were placed on ideal positions and refined with fixed isotropic displacement parameters using a riding model.

$\mathbf{10 \cdot py_2}$ crystallizes with half a benzene molecule (located on a 2-fold rotation axis) in the asymmetric unit.

Compounds **11** and **12** crystallize together in the same crystal. The site occupation factor of **11** refined to 0.734(4) and was fixed to 0.75 in order to avoid correlations between occupancy factors and displacement parameters. The 1,2 and 1,3 distances between the minor occupied C atoms were restrained to be equal, respectively, and these atoms were refined with a common isotropic displacement parameter. **11**/**12** crystallizes

with half a hexane molecule in the asymmetric unit, which is disordered about a center of inversion over two equally occupied sites.

13 crystallizes with half a hexane molecule in the asymmetric unit, located on a center of inversion. One of its CH_2 groups is disordered over two equally occupied sites.

CCDC reference numbers: 802380 (**9**), 802381 (9-*t*BuC(H)C(H)-9-borafluorene), 802382 (**10·py$_2$**), 802383 (**11**/**12**), 802384 (**13**), 802385 (**14**).

Computational Details. Geometry optimizations, analytic harmonic frequency analyses, and intrinsic reaction coordinate (IRC) calculations have been performed with the Gaussian09 program.[57] Initial geometry optimizations were performed employing the M06L functional[58] in combination with the small D95V basis.[59] To speed up the computations, we made use of the RI procedure[60] employing the DGA1 fitting basis[61] as implemented in Gaussian09. The resulting, rather moderate M06L/D95V/DGA1 level of density functional theory allowed for efficient explorations of potential reaction pathways, and it was found to provide very reasonable structures for minima and transition states. This level was also used for IRC calculations, which we performed to validate connectivities between minima and transition structures implied above. The resulting structures were subsequently reoptimized at the B3LYP(V)-D/TZVP level of DFT. In these calculations the B3LYP hybrid functional[62] was employed incorporating the VWN5 local correlation functional.[63] Empirical dispersion corrections devised by Grimme[64] were employed, and the TZVP basis set[65] was used. The resulting B3LYP(V)-D/TZVP level of density functional theory was recently identified as pleasingly accurate for related investigations.[66] The nature of all stationary points reported in the following has been characterized by the number of negative eigenvalues in the respective diagonalized force constant matrices (0 for minima, 1 for transition states; the wavenumbers of the imaginary modes of all transition states are given in the figures below). Unscaled zero-point vibrational energies as well as thermal and entropy corrections were obtained from computed Hessians using the standard procedures in Gaussian09 and were used to obtain Gibbs free energies, which relate to 298.15 K and ideal gas conditions (i.e, 0.04 mol l^{-1}).[67] All structures have been optimized within the highest possible molecular symmetry. All resulting nontrivial point groups are given in the figures below and all atoms involved in the chemical transformations have been highlighted by a ball-and-stick representation; all other hydrogen atoms have been omitted for clarity.

NMR isotropic shieldings σ were computed at the B97D/TZVP level of theory[64] within the GIAO[68] framework on structures reoptimized at this level of DFT. Tetramethylsilane ($\sigma(^1H) = 31.73$, $\sigma(^{13}C) = 182.96$) was chosen as internal standard to calculate the ^1H and ^{13}C chemical shift values δ. Diborane(6) ($\sigma(^{11}B) = 85.78$) was chosen as internal standard to calculate $\delta(^{11}B)$; the values obtained were corrected for the experimentally used standard $BF_3\cdot OEt_2$ ($\delta(B_2H_6) = 18.0$ ppm vs $BF_3\cdot OEt_2$). We validated this method by comparison of computed and measured ^1H, ^{13}C, and ^{11}B chemical shifts for compounds **5·py**, **6**, **8**, **9**, and **14** and found very good agreement within 0.08 ± 0.32 ppm (^1H), −0.7 ± 1.6 ppm (^{13}C), and −3.1 ± 3.4 ppm (^{11}B, mean signed deviations).

■ ASSOCIATED CONTENT

Supporting Information. Synthesis and NMR spectra of $(\mathbf{5})_2$, **5·py**, and 9-*t*BuC(H)C(H)-9-borafluorene. Crystallographic data of **9**, 9-*t*BuC(H)C(H)-9-borafluorene, **10·py$_2$**, **11**/**12**, **13**, and **14**. X-ray crystal structure analysis of 9-*t*BuC(H)C(H)-9-borafluorene. Quantum chemical results for pyridine adducts of **A** and **D**, reaction pathways for the *B*−*H*/*B*−*C* addition of **A** to **D**, free energies of oligomers **X**, **X^2**, and **X^3**, computed NMR shifts for **G**, **C**, **H**, **A·py**, **ABr**, **Ac**, and **A$_2$tBE**, tables with detailed computational results for all stationary points localized, as well as the full citation of reference 57. This material is available free of charge via the Internet at http://pubs.acs.org.

■ AUTHOR INFORMATION

Corresponding Author
Matthias.Wagner@chemie.uni-frankfurt.de; Max.Holthausen@chemie.uni-frankfurt.de

■ ACKNOWLEDGMENT

M.W. and M.C.H. gratefully acknowledge financial support by the Beilstein-Institut, Frankfurt/Main, Germany, within the research collaboration NanoBiC. A.H. is grateful to the Fonds der Chemischen Industrie (FCI) for a Ph. D. grant.

■ REFERENCES

(1) (a) Müllen, K; Wegner, G. *Electronic Materials: The Oligomer Approach*, Wiley-VCH, Weinheim, 1998. (b) Müllen, K; Scherf, U. *Organic Light-Emitting Devices: Synthesis Properties and Applications*, Wiley-VCH, Weinheim, 2005. (c) Müller, T. J. J.; Bunz, U. H. F. (Eds.) *Functional Organic Materials: Syntheses, Strategies and Applications*, Wiley-VCH, Weinheim, 2006.
(2) Entwistle, C. D.; Marder, T. B. *Angew. Chem., Int. Ed.* **2002**, *41*, 2927–2931.
(3) Entwistle, C. D.; Marder, T. B. *Chem. Mater.* **2004**, *16*, 4574–4585.
(4) Yamaguchi, S.; Wakamiya, A. *Pure Appl. Chem.* **2006**, *78*, 1413–1424.
(5) Doi, H.; Kinoshita, M.; Okumoto, K.; Shirota, Y. *Chem. Mater.* **2003**, *15*, 1080–1089.
(6) Jia, W. L.; Feng, X. D.; Bai, D. R.; Lu, Z. H.; Wang, S.; Vamvounis, G. *Chem. Mater.* **2005**, *17*, 164–170.
(7) Hudnall, T. W.; Chiu, C.-W.; Gabbaï, F. P. *Acc. Chem. Res.* **2009**, *42*, 388–397.
(8) Wade, C. R.; Broomsgrove, A. E. J.; Aldridge, S.; Gabbaï, F. P. *Chem. Rev.* **2010**, *110*, 3958–3984.
(9) Jäkle, F. *Coord. Chem. Rev.* **2006**, *250*, 1107–1121.
(10) Jäkle, F. *Chem. Rev.* **2010**, *110*, 3985–4022.
(11) Matsumi, N.; Naka, K.; Chujo, Y. *J. Am. Chem. Soc.* **1998**, *120*, 10776–10777.
(12) Scheibitz, M.; Bats, J. W.; Bolte, M.; Lerner, H.-W.; Wagner, M. *Organometallics* **2004**, *23*, 940–942.
(13) Sundararaman, A.; Victor, M.; Varughese, R.; Jäkle, F. *J. Am. Chem. Soc.* **2005**, *127*, 13748–13749.
(14) Heilmann, J. B.; Scheibitz, M.; Qin, Y.; Sundararaman, A.; Jäkle, F.; Kretz, T.; Bolte, M.; Lerner, H.-W.; Holthausen, M. C.; Wagner, M. *Angew. Chem., Int. Ed.* **2006**, *45*, 920–925.
(15) Niu, W.; Smith, M. D.; Lavigne, J. J. *J. Am. Chem. Soc.* **2006**, *128*, 16466–16467.
(16) Li, H.; Jäkle, F. *Angew. Chem., Int. Ed.* **2009**, *48*, 2313–2316.
(17) Scheibitz, M.; Li, H.; Schnorr, J.; Sánchez Perucha, A.; Bolte, M.; Lerner, H.-W.; Jäkle, F.; Wagner, M. *J. Am. Chem. Soc.* **2009**, *131*, 16319–16329.
(18) Cui, C.; Heilmann-Brohl, J.; Sánchez Perucha, A.; Thomson, M. D.; Roskos, H. G.; Wagner, M.; Jäkle, F. *Macromolecules* **2010**, *43*, 5256–5261.
(19) Matsumi, N.; Naka, K.; Chujo, Y. *J. Am. Chem. Soc.* **1998**, *120*, 5112–5113.
(20) Matsumi, N.; Miyata, M.; Chujo, Y. *Macromolecules* **1999**, *32*, 4467–4469.
(21) Matsumi, N.; Chujo, Y.; Lavastre, O.; Dixneuf, P. H. *Organometallics* **2001**, *20*, 2425–2427.
(22) Miyata, M.; Chujo, Y. *Polym. Bull.* **2003**, *51*, 9–16.
(23) Lorbach, A.; Bolte, M.; Li, H.; Lerner, H.-W.; Holthausen, M. C.; Jäkle, F.; Wagner, M. *Angew. Chem., Int. Ed.* **2009**, *48* 4584–4588.

(24) Lorbach, A.; Bolte, M.; Lerner, H.-W.; Wagner, M. *Chem. Commun.* **2010**, *46*, 3592–3594.
(25) Lorbach, A.; Bolte, M.; Lerner, H.-W.; Wagner, M. *Organometallics* **2010**, *29*, 5762–5765.
(26) Eisch, J. J.; Galle, J. E.; Kozima, S. *J. Am. Chem. Soc.* **1986**, *108*, 379–385.
(27) For selected recent references on the synthesis, structural peculiarities, and applications of boroles, see: (a) Braunschweig, H.; Fernández, I.; Frenking, G.; Kupfer, T. *Angew. Chem., Int. Ed.* **2008**, *47*, 1951–1954. (b) So, C.-W.; Watanabe, D.; Wakamiya, A.; Yamaguchi, S. *Organometallics* **2008**, *27*, 3496–3501. (c) Fan, C.; Piers, W. E.; Parvez, M. *Angew. Chem., Int. Ed.* **2009**, *48*, 2955–2958. (d) Huynh, K.; Vignolle, J.; Tilley, T. D. *Angew. Chem., Int. Ed.* **2009**, *48*, 2835–2837.
(28) Chase, P. A.; Piers, W. E.; Patrick, B. O. *J. Am. Chem. Soc.* **2000**, *122*, 12911–12912.
(29) Romero, P. E.; Piers, W. E.; Decker, S. A.; Chau, D.; Woo, T. K.; Parvez, M. *Organometallics* **2003**, *22*, 1266–1274.
(30) Grigsby, W. J.; Power, P. P. *J. Am. Chem. Soc.* **1996**, *118*, 7981–7988.
(31) Wehmschulte, R. J.; Khan, M. A.; Twamley, B.; Schiemenz, B. *Organometallics* **2001**, *20*, 844–849.
(32) For experimental as well as theoretical studies on 9-borafluorene-containing materials, see: (a) Yamaguchi, S.; Shirasaka, T.; Akiyama, S.; Tamao, K. *J. Am. Chem. Soc.* **2002**, *124*, 8816–8817. (b) Brière, J.-F.; Côté, M. *J. Phys. Chem. B.* **2004**, *108*, 3123–3129. (c) Thanthiriwatte, K. S.; Gwaltney, S. R. *J. Phys. Chem. A.* **2006**, *110*, 2434–2439. (d) Doskocz, J.; Doskocz, M.; Roszak, S.; Soloducho, J.; Leszczynski, J. *J. Phys. Chem. A.* **2006**, *110*, 13989–13994. (e) Wakamiya, A.; Mishima, K.; Ekawa, K.; Yamaguchi, S. *Chem. Commun.* **2008**, 579–581. (f) Bonifácio, V. D. B.; Morgado, J.; Scherf, U. *J. Polym. Sci., Part A: Polym. Chem.* **2008**, *46*, 2878–2883. (g) Muhammad, S.; Janjua, M. R. S. A.; Su, Z. *J. Phys. Chem. C* **2009**, *113*, 12551–12557.
(33) Hong, H.; Chung, T. C. *J. Organomet. Chem.* **2004**, *689*, 58–64.
(34) Köster, R.; Willemsen, H.-G. *Liebigs Ann. Chem.* **1974**, 1843–1850.
(35) 9-H-9-Borafluorene derivatives bearing bulky substituents at their phenylene rings have been suggested (i) as reaction intermediate during the reduction of 2,6-(2,4,6-*i*Pr$_3$C$_6$H$_2$)$_2$C$_6$H$_3$BBr$_2$ with KC$_8$ (cf. Ref 30) and (ii) as transient product of an intramolecular C-H activation of the terphenylborane {2,6-(4-*t*BuC$_6$H$_4$)$_2$C$_6$H$_3$BH(μ-H)}$_2$ (cf. Wehmschulte, R. J.; Diaz, A. A.; Khan, M. A. *Organometallics* **2003**, *22*, 83–92.
(36) van Veen, R.; Bickelhaupt, F. *J. Organomet. Chem.* **1973**, *47*, 33–38.
(37) Knizek, J.; Nöth, H. *J. Organomet. Chem.* **2000**, *614*−*615*, 168–187.
(38) Köster, R.; Benedikt, G. *Angew. Chem.* **1963**, *75*, 419.
(39) Kaufmann, L.; Vitze, H.; Bolte, M.; Lerner, H.-W.; Wagner, M. *Organometallics* **2008**, *27*, 6215–6221.
(40) Gross, U.; Kaufmann, D. *Chem. Ber.* **1987**, *120*, 991–994.
(41) Wakamiya, A.; Mishima, K.; Ekawa, K.; Yamaguchi, S. *Chem. Commun.* **2008**, 579–581.
(42) Hübner, A.; Lerner, H.-W.; Wagner, M.; Bolte, M. *Acta Crystallogr.* **2010**, *E66*, o444.
(43) Wrackmeyer, B. *Prog. Nucl. Magn. Reson. Spectrosc.* **1979**, *12*, 227–259.
(44) Nöth, H.; Wrackmeyer, B. *Nuclear Magnetic Resonance Spectroscopy of Boron Compounds*. In *NMR Basic Principles and Progress*; Diehl, P., Fluck, E., Kosfeld, R., Eds.; Springer: Berlin, Heidelberg, New York, 1978.
(45) Wrackmeyer, B.; Thoma, P.; Kempe, R.; Glatz, G. *Collect. Czech. Chem. Commun.* **2010**, *75*, 743–756.
(46) Piers, W. E.; Irvine, G. J.; Williams, V. C. *Eur. J. Inorg. Chem.* **2000**, 2131–2142.
(47) Katz, H. E. *J. Org. Chem.* **1985**, *50*, 5027–5032.
(48) Spence, R. E. v. H.; Piers, W. E.; Sun, Y.; Parvez, M.; MacGillivray, L. R.; Zaworotko, M. J. *Organometallics* **1998**, *17*, 2459–2469.
(49) Kessler, S. N.; Wegner, H. A. *Org. Lett.* **2010**, *12*, 4062–4065.
(50) Hoefelmeyer, J. D.; Gabbaï, F. P. *J. Am. Chem. Soc.* **2000**, *122*, 9054–9055.
(51) Narula, C. K.; Nöth, H. *Inorg. Chem.* **1985**, *24*, 2532–2539.
(52) A structure plot of **14** is already shown in ref 34, however, the crystal data have never been published. We have therefore performed a full X-ray crystal structure analysis of the compound.
(53) We are aware of only one other compound featuring a comparable B-(μ-aryl)-B structural motif: Pilz, M.; Allwohn, J.; Massa, W.; Berndt, A. *Angew. Chem., Int. Ed. Engl.* **1990**, *29*, 399–401.
(54) Hofmann, M.; Scheschkewitz, D.; Ghaffari, A.; Geiseler, G.; Massa, W.; Schaefer, H. F., III; Berndt, A. *J. Mol. Mod.* **2000**, *6*, 257–271.
(55) Sheldrick, G. M. *Acta Crystallogr.* **1990**, *A46*, 467–473.
(56) Sheldrick, G. M. *SHELXL-97. A Program for the Refinement of Crystal Structures*. Universität Göttingen, Göttingen, 1997.
(57) Frisch, M. J. et al. *Gaussian 09, Revision A.02*, Gaussian, Inc.: Wallingfort CT, 2009.
(58) Zhao, Y.; Truhlar, D. G. *J. Chem. Phys.* **2006**, *125* (194101), 1–18.
(59) Dunning Jr., T. H.; Hay, P. J. in *Modern Theoretical Chemistry*. Ed. Schaefer III, H. F. Vol. 3, 1−28; Plenum: New York, 1976.
(60) (a) Eichkorn, K.; Treutler, O.; Öhm, H.; Häser, M.; Ahlrichs, R. *Chem. Phys. Lett.* **1995**, *240*, 283–289. (b) Kendall, R. A.; Früchtl, H. A. *Theor. Chem. Acc.* **1997**, *97*, 158–163. (c) Dunlap, B. I. *J. Mol. Struct. (THEOCHEM)* **2000**, *529*, 37–40. (d) Dunlap, B. I. *J. Chem. Phys.* **1983**, *78*, 3140–3142. (e) Eichkorn, K.; Weigend, F.; Treutler, O.; Ahlrichs, R. *Theor. Chem. Acc.* **1997**, *97*, 119–124.
(61) Godbout, N.; Salahub, D. R.; Andzelm, J.; Wimmer, E. *Can. J. Chem.* **1992**, *70*, 560–571.
(62) (a) Becke, A. D. *Phys. Rev. A* **1988**, *38*, 3098–3100. (b) Lee, C.; Yang, W.; Parr, R. G. *Phys. Rev. B* **1988**, *37*, 785–789. (c) Stephens, P. J.; Devlin, F. J.; Chabalowski, C. F.; Frisch, M. J. *J. Phys. Chem.* **1994**, *98*, 11623–11627. (d) Becke, A. D. *J. Chem. Phys.* **1993**, *98*, 5648–5652.
(63) (a) Vosko, S. H.; Wilk, L.; Nusair, M. *Can. J. Phys.* **1980**, *58*, 1200–1211. (b) Hertwig, R. H.; Koch, W. *Chem. Phys. Lett.* **1997**, *268*, 345–351.
(64) Grimme, S. *J. Comput. Chem.* **2006**, *27*, 1787–1799.
(65) (a) Schäfer, A.; Horn, H.; Ahlrichs, R. *J. Chem. Phys.* **1992**, *97*, 2571–2577. (b) Schäfer, A.; Huber, C.; Ahlrichs, R. *J. Chem. Phys.* **1994**, *100*, 5829–5835.
(66) Rakow, J. R.; Tüllmann, S.; Holthausen, M. C. *J. Phys. Chem. A* **2009**, *113*, 12035–12043.
(67) McQuarrie, D. A.; Simon, J. D. *Physical Chemistry* − *A Molecular Approach*. University Science Books: Sausalito, CA, 1997.
(68) (a) Ditchfield, R. *Mol. Phys.* **1974**, *27*, 789–807. (b) Wolinski, K.; Hinton, J. F.; Pulay, P. *J. Am. Chem. Soc.* **1990**, *112*, 8251–8260.